Multistep Energy and Electron Transfer Processes in Novel Rotaxane Donor–Acceptor Hybrids Generating Microsecond Lived Charge Separated States

Journal:	*Chemical Science*
Manuscript ID	SC-EDG-08-2015-002895.R1
Article Type:	Edge Article
Date Submitted by the Author:	14-Sep-2015
Complete List of Authors:	Kirner, Sabrina; Friedrich-Alexander-Universitat Erlangen-Nurnberg, Department of Chemistry Guldi, Dirk; University of Erlangen-Nűrnberg, Department of Chemistry and Pharmacy Henkel, Christian; Friedrich-Alexander-Universitat Erlangen-Nurnberg, Department of Chemistry Megiatto Jr., Jackson; New York University, Chemistry Schuster, David; New York University, Department of Chemistry

SCHOLARONE™
Manuscripts

Electronic Supporting Information

Multistep Energy and Electron Transfer Processes in Novel Rotaxane Donor–Acceptor Hybrids Generating Microsecond Lived Charge Separated States

Sabrina V. Kirner, [a] Christian Henkel[a], Dirk M. Guldi, [*a] Jackson D. Megiatto, Jr.[b†] and David I. Schuster*[b]

[a] Department of Chemistry and Pharmacy and Interdisciplinary Center for Molecular Materials, Friedrich-Alexander-Universität Erlangen-Nürnberg, Egerlandstrasse 3, 91058 Erlangen, Germany
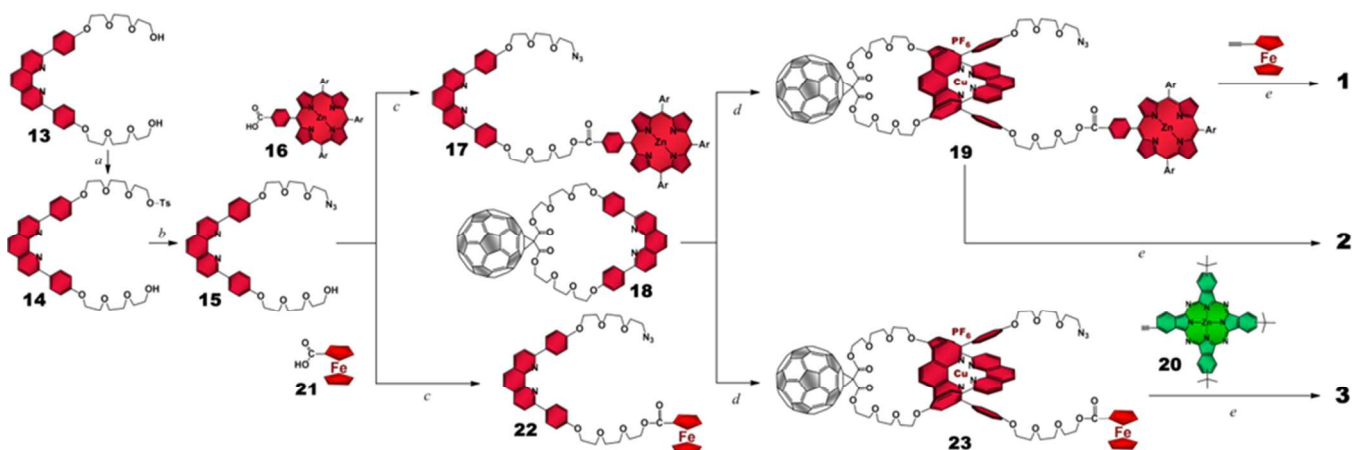
[b] Department of Chemistry, New York University, New York, *NY 10003, USA.*

[†] Present Address: Institute of Chemistry, University of Campinas, PO Box 6154, Campinas, SP, 13084-861, Brazil.

1. Supplementary Figures

Scheme S1 Convergent synthetic strategy adopted to prepare target rotaxanes **1**, **2**, and **3**.

(a) tosyl chloride, dichloromethane, $0^{\circ}C$ for 4 h then rt for 12 h, 45% yield; *(b)* sodium azide, dimethylformamide, $80^{\circ}C$, 12 h, 90% yield; *(c)* 1-ethyl-3-(3-dimethylaminopropyl)carbodiimide (EDC), dimethylaminopyridine (DMAP), dichloromethane, rt, 12 h, 85% yield; *(d)* $Cu(CH_3CN)_4][PF_6]$, dichloromethane/acetonitrile (7:3, v/v), rt, 12 h, quantitative (by TLC); *(e)* copper iodide, sodium ascorbate, sulfonated bathophenathroline, 1,8-Diazabicycloundec-7-ene (DBU), dichloromethane/water/ethanol (1:1:1, v/v), $70^{\circ}C$, 12 h. Ar = 3,5-di-*tert*-butylphenyl.

2. Structural Characterization

2.1. MALDI-TOF Mass Spectrometry

MALDI-TOF analysis in positive mode for all rotaxanes revealed the expected ion mass peak corresponding to the molecular mass of the rotaxanes lacking the PF_6^- counter-ion as well as the classical fragmentation pattern observed for $[Cu(phen)_2]^+$-based interlocked systems upon ionization.[1-4] For example, a MALDI-TOF spectrum of rotaxane **2** (Figure S1) clearly reveals the ion mass peak at m/z 3939.9 (rotaxane **2** - PF_6) corresponding to the proposed rotaxane structure. The latter comes along with two extra ion mass peaks both with high intensity. These peaks correspond to a fragment lacking the fullerene (m/z 3219.4), suggesting rupture of the cyclopropane moiety that links the carbon cage to the phen-macrocycle, and to the thread component coordinated to a Cu ion (m/z 2522.8), indicating further rupture and loss of the phen-macrocycle.
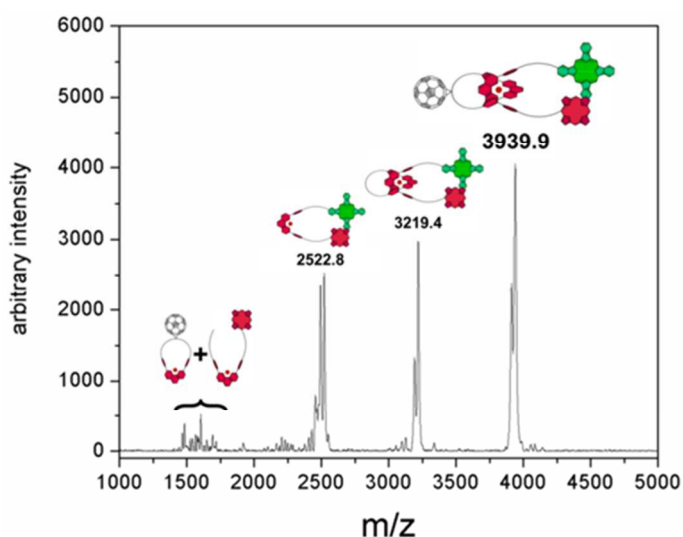
Fig. S1: MALDI-TOF mass spectrum of rotaxane **2**. Positive mode, α-cyano-4-hydroxycinnamic acid (CCA) used as matrix.

It is interesting to note that the ion mass peak at m/z 3219.4 appears as doublets, while the peak at m/z 2522.8 appears as a triplet. The doublets have a difference of m/z 28, while the triplet signal has a difference of m/z 28 and 62. We propose that the extra peaks that appear at m/z 28 units lower in the MALDI spectrum correspond to species that had lost a single N_2 molecule due to fragmentation of the triazole ring upon ionization.[5, 6] The species detected at m/z 62 units lower corresponds to the protonated thread fragment lacking the Cu ion. The minor peaks in the MALDI spectrum likely correspond to unusual fragments of the rotaxane structure since increasing the laser power during the MALDI experiments increases the intensity of those minor peaks while sig-

nificantly decreasing the peak corresponding to rotaxane **2**. Similar MALDI spectra were obtained for rotaxanes **1** and **3**.

2.2. ^{1}H Nuclear Magnetic Resonance – NMR

^{1}H NMR investigation revealed that rotaxanes **1**, **2**, and **3** are very flexible structures existing in several interconverting conformations with complex dynamics on the NMR time scale. It is safe to assume that they are driven by secondary interactions between the chromophores.[1, 2, 7-13] Variable temperature ^{1}H NMR studies on rotaxane **1** in DMF-d_7 showed increasing broadening of the peaks at lower temperatures with no coalescence even at temperatures as low as 233 K. A somewhat cleaner spectrum was obtained at 100°C, which allowed us to identify key protons of the proposed structure, namely the pyrrolic protons of the porphyrin between 8.92 and 8.86 ppm, the triazole proton at 8.05 ppm, and the ferrocene nuclei[10, 14] at 4.71, 4.33 and 4.01 ppm as well as the protons attached to the phenyl rings linked to positions 2 and 9 of the phen moieties, which appears in the usual upfield region at 7.42, 7.22, 6.18, 6.09 ppm, confirming that the two phen groups are entwined around the Cu(I) template ion.[15] For rotaxanes **2** and **3**, which bear phthalocyanines, aggregation is evident in the ^{1}H NMR spectra even at high temperatures. Although some key features of the proposed rotaxane structures can be safely assigned, the signals are unfortunately too broad for a detailed analysis.

3.   Ground State Interactions
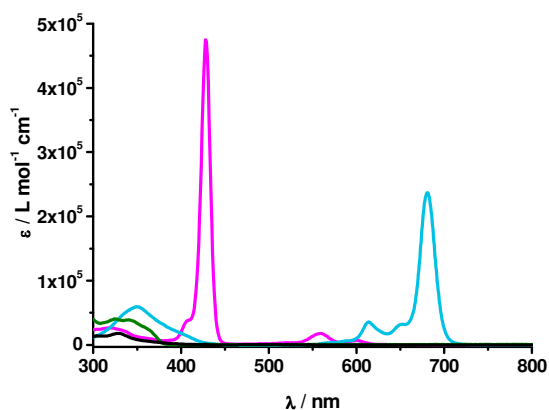
3.1. Electrochemistry

To probe the redox properties of the electron donor-acceptor rotaxanes (**1**-**3**) as well as the corresponding reference compounds (**4**-**12**) square wave voltammetry and differential pulse voltammetry experiments were carried out in dichloromethane (DCM) in the presence of 0.1 M tetrabutylammonium hexafluorophosphate (TBAFPF$_6$) as supporting electrolyte and ferrocene/ferrocenium as internal reference. Table S1 summarizes the electrochemical data with all redox potentials reported in volts (V) relative to the ferrocene couple (Fc/Fc+).

While the C$_{60}$ reference **10** was inactive under oxidative conditions, one-electron reductions were observed at −1.06 and −1.44 V resembling the trend found for pristine C$_{60}$.[16-18] Due to the partial loss of π-conjugation, **10** reveals a shift towards more negative reductions when compared to pristine C$_{60}$. ZnTPP (**11**) exhibits one-electron oxidations at +0.28 and +0.62 V. Zn^{t}Bu$_4$Pc (**12**) features only one oxidation at +0.22 eV within the electrochemical window. Catenane **9** reveals a single oxidation at +0.16 V, which correlates with the one-electron oxidation of the copper center, namely [Cu(phen)$_2$]$^+$/[Cu(phen)$_2$]$^{2+}$.[1, 7] C$_{60}$-[Cu(phen)$_2$]$^+$ catenane **8** shows two one electron reductions at −1.12 and −1.48 V, corresponding to C$_{60}$ centered processes. In addition, the one-electron oxidation of [Cu(phen)$_2$]$^+$ evolves at +0.16 V. To this end, the presence of C$_{60}$ has no notable impact on the [Cu(phen)$_2$]$^+$ oxidation. Reference thread **5** features two oxidations at +0.26 and +0.62 V, corresponding to the oxidation of ZnP. A third oxidation at -0.01 V assigned to the ferrocene oxidation is shifted by 0.01 V to lower potentials compared to the ferrocene reference. In rotaxane **4**, three oxidations are discernible. The first oxidation at +0.03 V is assigned to a ferrocene centered process. The second oxidation at +0.28 V is twice in intensity when compared to the one at +0.03 V. Thus, we hypothesize that it corresponds to the coalescence of a [Cu(phen)$_2$]$^+$ as well as a ZnP oxidation.[1] Finally, the third oxidation at +0.88 V, which relates to the second oxidation of ZnP, is shifted towards more positive potentials when compared to ZnTPP and reference **11**. It is likely that the presence of [Cu(phen)$_2$]$^+$ impacts the ZnP oxidation. Thread reference **7** is inactive under reductive conditions. Under oxidative conditions, two oxidations are discernible for **7** at +0.21 and +0.75 V. Considering that the former is broader and more intense, we assume that it is a superimposition of the first ZnP oxidation and the first ZnPc oxidation. The second oxidation is assigned to the second oxidation of ZnP. A similar conclusion is derived for reference **6**. Here, the first oxidations of ZnP, ZnPc, and [Cu(phen)$_2$]$^+$ cannot be clearly resolved at about +0.20 V, while the second ZnP oxidation sets in at ~0.7 V. No reduction peaks were observed within the electrochemical window of DCM.

Table S1 Oxidation and reduction potentials. All redox potentials reported in volts (V) are relative to the ferrocene couple (Fc/Fc$^+$) as internal reference. Electrolyte: 0.1 M TBAFPF$_6$ in dichloromethane (DCM) or *ortho*-dichlorobenzene (*o*-DCB). P = porphyrin and Pc = phthalocyanine.

	Solvent	Oxidation					Reduction	
		$P^{\bullet+}/P^{2+}$	$P/P^{\bullet+}$	$Pc/Pc^{\bullet+}$	Cu^+/Cu^{2+}	Fc/Fc^+	$C_{60}/C_{60}^{\bullet-}$	$C_{60}^{\bullet-}/C_{60}^{2-}$
1	DCM	0.88	0.24	–	0.24	0.04	−1.09	−1.45
2	DCM	20	0.18	0.18	0.13	–	−1.13	−1.54
3	DCM	–	–	0.18	0.18	−0.05	−1.10	−1.55
4	DCM	0.88	0.28	–	0.28	0.03	–	–
5	DCM	0.61	0.26	–	–	−0.01	–	–
6	DCM	0.74	0.20	0.20	0.20	–	–	–
7	DCM	0.75	0.21	0.21	–	–	–	–
8[1]	*o*-DCB	–	–	–	0.16	–	−1.12	−1.48
9[10]	*o*-DCB	–	–	–	0.16	–	–	–
10	DCM	–	–	–	–	–	−1.06	−1.44
11	*o*-DCB	0.62	0.28	–	–	–	–	–
12	DCM	–	–	0.22	–	–	–	–

3.2 UV-vis Absorption

Fig. S2 UV/Vis absorption spectra of reference compounds **9** (olive), C$_{60}$ reference **10** (black), ZnTPP **11** (magenta) and ZnPc **12** (cyan) in PhCN.
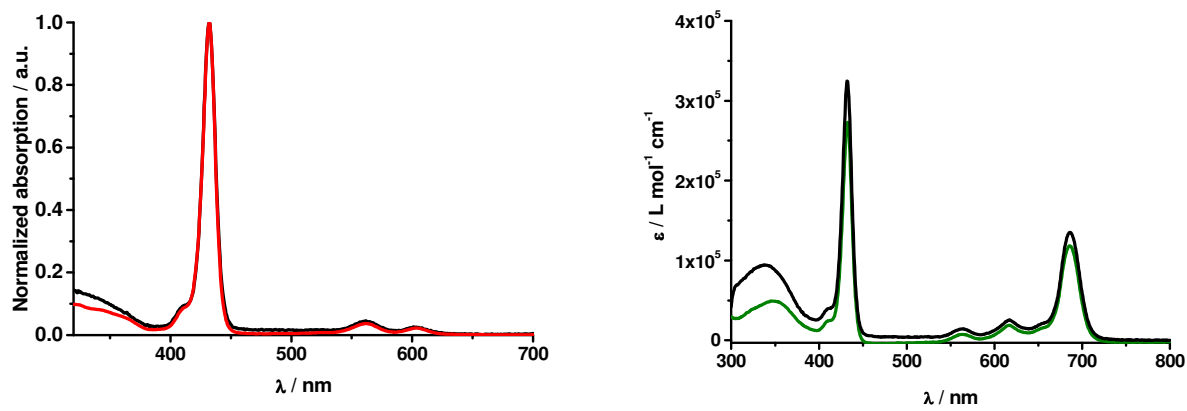
Fig. S3 Left: normalized UV/Vis absorption spectra of reference compounds **4** (black) and **5** (red) in PhCN. Right: UV/Vis absorption spectra of reference compounds **6** (black) and **7** (olive) in PhCN.

4. Excited State Interactions

4.1. Emission Spectroscopy

Table S2 Fluorescence parameters and fluorescence lifetimes in THF at 298 K in air-equilibrated solutions.[a]

Compound	λ_{exc} (nm)	Excited State	λ_{max} (nm)	τ (ns)	Φ_F	E_{00} (eV)
1	420	Fc–**ZnP***–[Cu(phen)$_2$]$^+$–C$_{60}$	602	0.82	0.02	2.06
	320	Fc–ZnP–**[Cu(phen)$_2$]$^+$***-C$_{60}$	755	–	3.6x10^{-4}	1.64
2	420	**ZnP***-ZnPc–[Cu(phen)$_2$]$^+$–C$_{60}$	602	< 0.15	0.006	2.06
	610	ZnP–**ZnPc***–[Cu(phen)$_2$]$^+$–C$_{60}$	686	1.7	0.12	1.81
3	610	Fc–**ZnPc***–[Cu(phen)$_2$]$^+$–C$_{60}$	679	2.1	0.15	1.83
4	420	Fc–**ZnP***–[Cu(phen)$_2$]$^+$	604	0.81	0.02	2.05
	320	Fc-ZnP–**[Cu(phen)$_2$]$^+$***	756	–	7.5x10^{-4}	1.64
5	420	Fc-**ZnP***-(phen)	603	1.8	0.04	2.06
6	420	**ZnP***-ZnPc–[Cu(phen)$_2$]$^+$	603	0.19	0.008	2.06
	610	ZnP-**ZnPc***–[Cu(phen)$_2$]$^+$	688	1.6	0.07	1.80
7	420	**ZnP***-ZnPc–(phen)	602	0.15	0.004	2.06
	610	ZnP-**ZnPc***–(phen)	686	2.3	0.13	1.81
8	320	**[Cu(phen)$_2$]$^+$***-C$_{60}$	765	–	2.5x10^{-4}	1.62
	350	[Cu(phen)$_2$]$^+$-**C$_{60}$***	710	–	2.3x10^{-5}	1.75
9[b]	320	**[Cu(phen)$_2$]$^+$***	759	2.5	4.8x10^{-3}	1.63
10	350	**^{1}*C$_{60}$-malonate**[d]	715	1.48	1.0x10^{-3}	1.73
11	420	**ZnTPP***	602	2.0	0.04	2.06
12	610	**ZnPc***	679	3.7	0.3	1.83

[a] λ_{max} = emission maxima; τ = fluorescence lifetime; Φ_F = fluorescence quantum yields; E_{00} = Energy of the corresponding excited state relative to the ground state, calculated from the emission maximum (λ_{max}); [b] from reference 3.
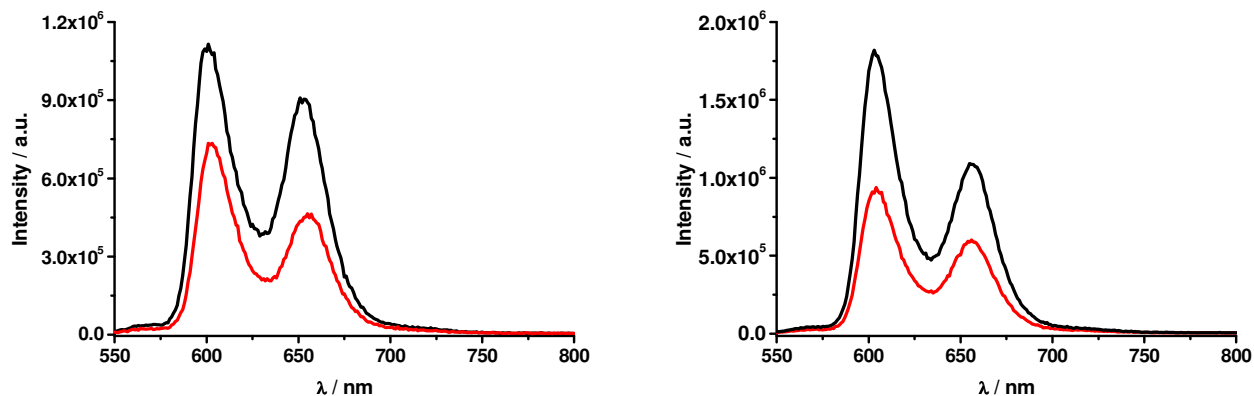
Fig. S4 Left: emission spectra of Fc-ZnP-[Cu(phen)$_2$]$^+$-C$_{60}$ **1** (red) and ZnTPP **11** (magenta) in THF upon excitation at 420 nm (OD = 0.045). Right: Emission spectra of reference compounds **4** (red) and **5** (black) in THF upon excitation at 420 nm (OD = 0.052).
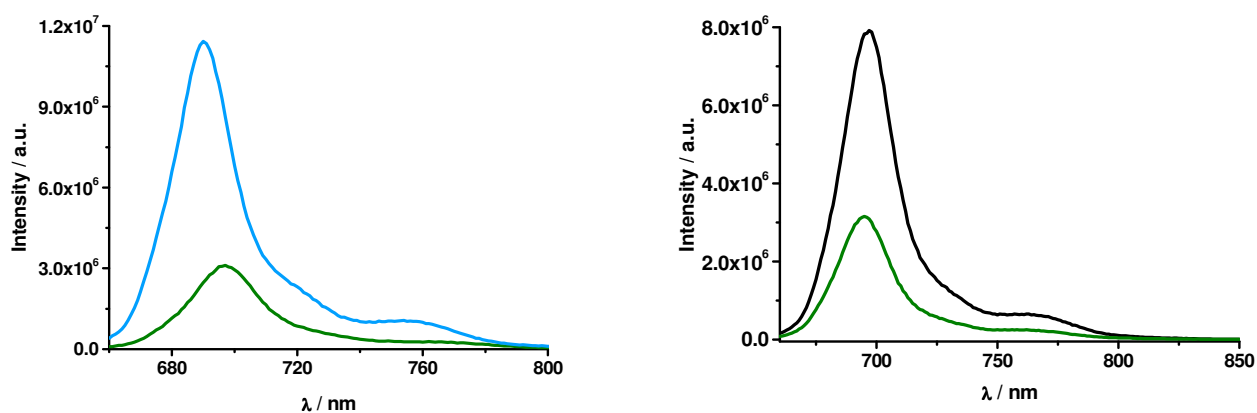
Fig. S5 Left: emission spectra of ZnP-ZnPc-[Cu(phen)$_2$]$^+$-C$_{60}$ **2** (olive) and Zn^{t}Bu$_4$Pc (cyan) in PhCN upon excitation at 650 nm (OD = 0.09); Right: emission spectra of reference compounds 5 (olive) and 6 (black) in PhCN upon excitation at 650 nm (OD = 0.06);
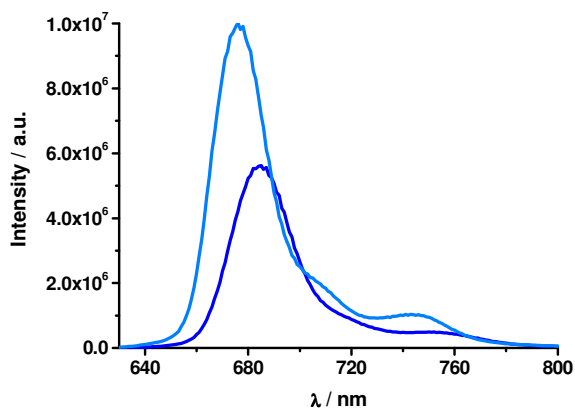
**Fig. S6** Emission spectra of ZnPc-Fc-[Cu(phen)$_2$]$^+$-C$_{60}$ **3** (blue) and the ZnPc reference **12** (cyan) in PhCN upon excitation at 610 nm (OD = 0.21).
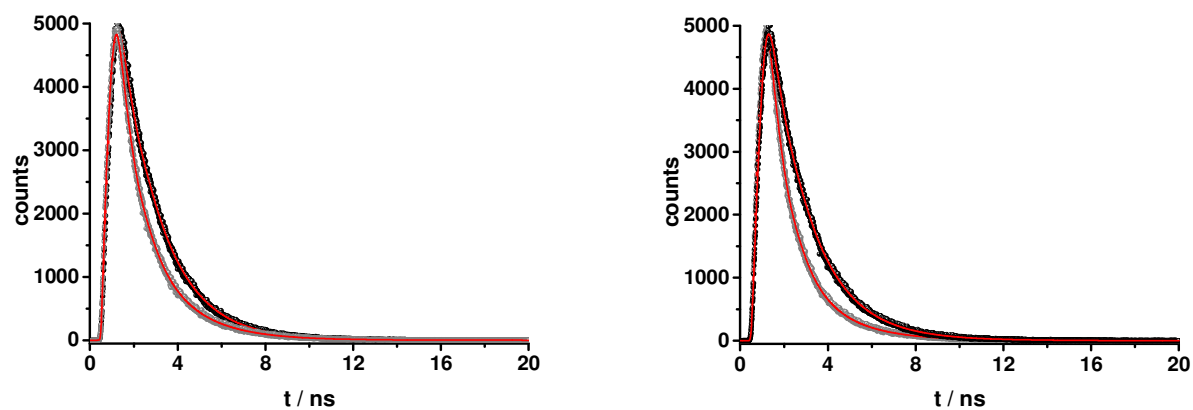
Fig. S7 Left: fluorescence decay of ZnTPP **11** (black) and Fc-ZnP-[Cu(phen)$_2$]$^+$-C$_{60}$ **1** (grey) and corresponding fits (red) upon excitation at 403 nm and detection at 600 nm in THF at RT. Right: fluorescence decay of reference compounds **5** (black) and **4** (grey) and corresponding fits (red) upon excitation at 403 nm and detection at 600 nm in THF at RT.
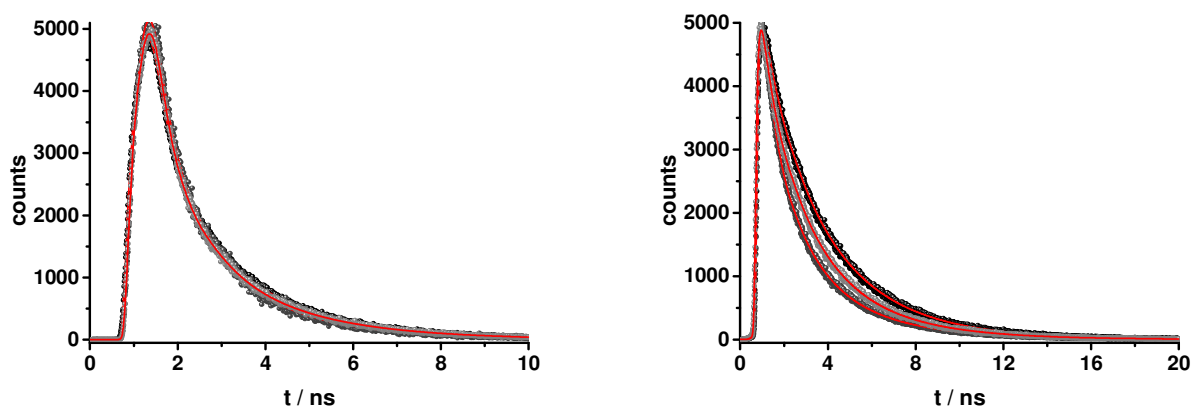
Fig. S8 Left: fluorescence decay of ZnP-ZnPc-[Cu(phen)$_2$]$^+$-C$_{60}$ **2** (grey), references **6** (dark grey) and **7** (grey)and corresponding fits (red) upon excitation at 403 nm and detection at 600 nm in THF at RT. Right: fluorescence decay of ZnP-ZnPc-[Cu(phen)$_2$]$^+$-C$_{60}$ **2** (grey), reference compounds **6** (dark grey) and **7** (grey) and corresponding fits (red) upon excitation at 647 nm and detection at 690 nm in THF at RT.
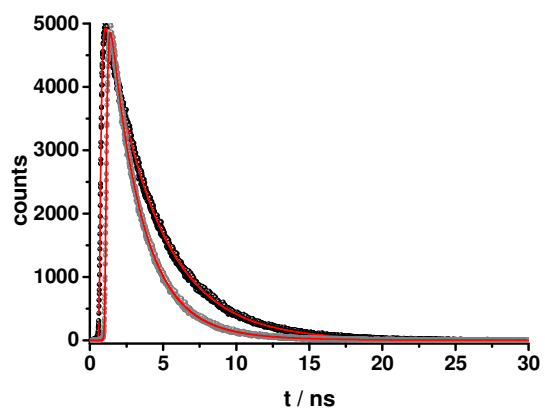
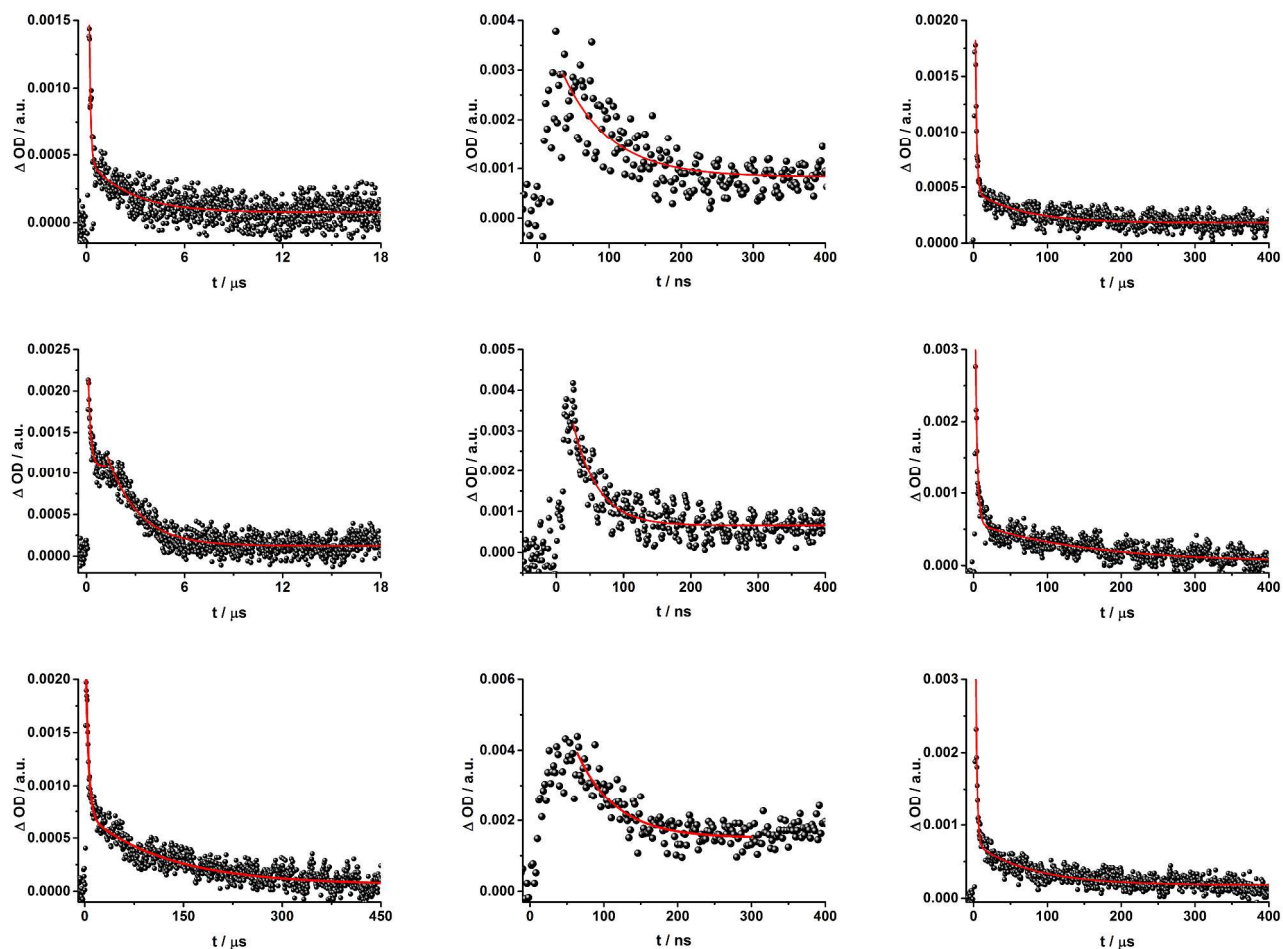**Fig. S9** Fluorescence decay of ZnPc **12** (black) and Fc-ZnPc-[Cu(phen)$_2$]$^+$-C$_{60}$ **3** (grey) and corresponding fits (red) upon excitation at 647 nm and detection at 680 nm in THF at RT.

4.2. Transient Absorption

Fig. S10 Time absorption profiles of Fc-ZnP-[Cu(phen)$_2$]$^+$-C$_{60}$ rotaxane 1 in tetrahydrofuran at room temperature under oxygen atmosphere (top), air (center) and argon atmosphere (bottom) at 680 nm (left) and 1010 nm (center and right), monitoring the charge recombination.

Table S3 Excited state lifetimes from ns transient absorption measurements on rotaxane **1** in THF under air, Ar and O$_2$ at room temperature.

	460 nm	680 nm			1010 nm	
O$_2$	111 ± 1 ns	110 ± 11 ns	2.5 ± 0.2 µs	67 ± 1 ns	2.1 ± 0.5 µs	60 ± 20 µs
Air	157 ± 19 ns	178 ± 21 ns	2.1 ± 0.3 µs	48 ± 3 ns	2.1 ± 0.1 µs	60 ± 12 µs
Ar	142 ± 12 µs	112 ± 14 µs	2.6 ± 0.1 µs	55 ± 3 ns	2.6 ± 0.1 µs	66 ± 8 µs
average	–	–	2.3 ± 0.3 µs	55 ± 8 ns	2.3 ± 0.4 µs	61 ± 16 µs
transient	^{3}ZnP*	^{3}ZnP*	ZnP$^{•+}$	C$_{60}$$^{•-}$	C$_{60}$$^{•-}$	C$_{60}$$^{•-}$

4.2.1. Reference compounds excited at 387 nm (fs-laser) and 355 nm (ns-laser)

The differential absorption spectra of C_{60} **10** are known from the literature.[3,5] Upon, for example, 387 nm fs-excitation the singlet excited state is formed immediately after the laser pulse with maxima at 510 and 920 nm. Within 1.7 ns the singlet excited state undergoes quantitative intersystem crossing to the energetically lower lying triplet excited state with a characteristic maximum at 720 nm. A triplet lifetime of 23 µs was determined upon 355 nm ns-excitation in argon saturated THF.

The differential absorption changes recorded upon 387 nm excitation of catenane **9** are dominated by characteristic MLCT transient absorptions. The latter include a broad maximum between 540 and 610 nm followed by another maximum around 910 nm. As a complement, transient bleaching at 440 and 700 nm corresponds to the MLCT absorption.[1, 8-11, 19] From the transient absorption changes a lifetime of 645 ns is derived upon ns-excitation and is attributed to the MLCT triplet excited state,[1] since it is well established that the MLCT singlet excited state transforms within hundreds of femtoseconds to the energetically lower lying MLCT triplet excited state.[20, 21]

Upon fs-excitation at 387 nm, the differential absorption spectra of **8** in THF are a combination of the transient changes recorded for references **9** and **10**. The transient observed at 590 nm is attributed to the ^{3*}MLCT, while the maxima at 530 and 920 nm correlate to the C_{60} singlet excited state. The latter decays rapidly with a lifetime of 40 ps due to the presence of $[Cu(phen)_2]^+$. The MLCT triplet excited state does not decay completely within the 7.5 ns time scale of our experimental setup. The peak at 1035 nm is the fingerprint absorption of the one-electron reduced C_{60}.[22] Thus, it is concluded that the deactivation of the C_{60} singlet excited state involves an electron transfer. The one-electron reduced form of C_{60} is stable on the time scale of the femtosecond experiments and decays in complementary ns-excitation experiments with a lifetime of 100 ns in THF.

For ZnPc **12** differential absorption changes evolve immediately after the 387 nm laser pulse, characterized by transient bleaching at 610 and 680 nm and an absorption maximum at 850 nm in THF, corresponding to the singlet excited state.[23] The latter decays within ~ 3 ns to populate the energetically lower-lying triplet excited state. The newly developing band at 480 nm reflects the diagnostic signature of the ZnPc triplet excited state with a lifetime of 120 µs.[23, 24]

4.2.2. Reference compounds excited at 420 nm (fs-laser)

ZnTPP **11** was excited with 420 nm fs-laser pulses. In this particular case, transient characteristics, which are formed immediately, include minima at 420, 560, and 600 nm, a maximum at 460 nm, and a broad absorption from 570 to 750 nm in THF. These correspond to the singlet excited state of ZnP.[1] Within 2 ns the ZnP singlet

excited state decays to the energetically lower lying ZnP triplet state with a 840 nm maximum and a 45 µs life-time.[25,1]

When exciting **5** into the ZnP Soret band at 420 nm the visible part of the spectrum is dominated by the ZnP singlet excited state with maxima at 455, 580, and 635 nm and ground state bleaching with minima at 425, 560, and 600 nm. Here, the ZnP singlet excited state undergoes intersystem crossing within 1.7 ns to yield maxima at 470 and 850 nm. The lifetime of the latter exceeds the 7.5 ns time scale of the experimental setup.
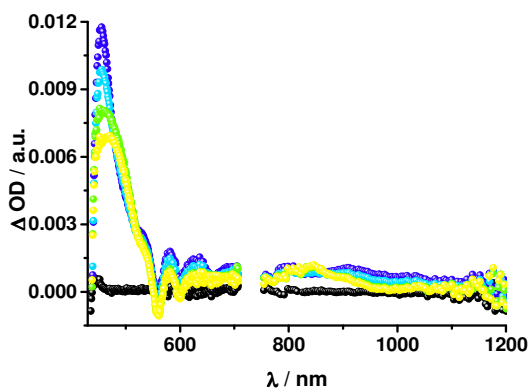
Fig. S11 Transient absorption spectrum (visible and near-infrared) of ZnP-Fc-(phen) reference **5** registered upon femtosecond flash photolysis (420 nm; 150 nJ) in THF with time delays between 0 (black) and 7.5 (yellow) ns at room temperature.

4.2.3. Reference compounds excited at 387 / 420 nm (fs-laser) and 425 nm (ns-laser)

Rotaxane **4** was excited at either 420 or at 387 nm. With the 420 nm excitation wavelength ZnP is mainly excited, while at 387 nm ZnP and $[Cu(phen)_2]^+$ both absorb. Still, excitation at either wavelength results in spectra, which are dominated by the characteristic ZnP signatures, as seen for model **5**. The ZnP singlet excited state decays via ISC within ~ 800 ps to give the triplet excited state of ZnP with its 460 and 850 nm absorption characteristics is discernable (Figure 6, right). Upon comparison with **5**, the rather broad transient in the near infrared is assigned to the MLCT triplet excited state. Considering that in **4** the ZnP singlet excited state lifetime is notably reduced relative to **5** we conclude that the presence of $[Cu(phen)_2]^+$ induces ZnP fluorescence quenching via energy transfer. However, no evidence was found in support of an electron transfer process. Thus, we conclude that energy transfer to $[Cu(phen)_2]^+$ dominates the excited state deactivation of ZnP in rotaxane **4**.
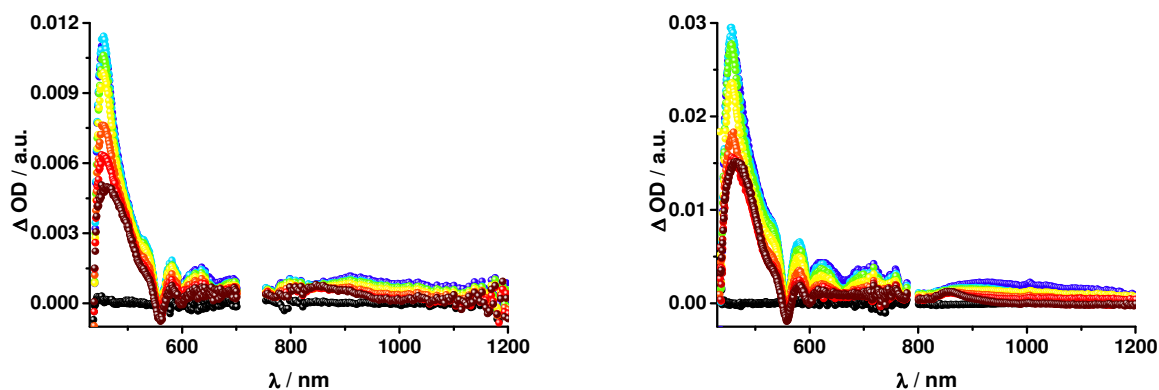
Fig. S12 Left: Transient absorption spectrum (visible and near-infrared) registered upon femtosecond flash photolysis (420 nm, 150 nJ) of ZnP-Fc-[Cu(phen)$_2$] rotaxane **3** in THF with time delays between 0 (black) and 7500 (wine) ps at room temperature. Right: Transient absorption spectrum (visible and near-infrared) registered upon femtosecond flash photolysis (387 nm, 200 nJ) of ZnP-Fc-[Cu(phen)$_2$] rotaxane **3** in THF with time delays between 0 (black) and 7500 (wine) ps at room temperature.

4.2.4. References excited at 387 / 420 / 660 nm (fs-laser) and 425 / 670 nm (ns-laser)

Upon exclusive excitation of ZnPc of ZnPc-phen-ZnP thread **7** at 660 nm the differential absorption spectra feature only ZnPc transients, namely its singlet excited state at ~ 800 nm with a lifetime 2.9 ns in THF and its triplet excited state at 490 nm including ground state bleaching at 680 nm.[24, 26-31] In contrast, upon excitation of **7** at 420 nm, which matches the ZnP Soret band, the visible part of the spectrum is dominated by the ZnP signature absorptions. The 450 nm ZnP singlet excited state undergoes energy transfer within 50 ps to yield the ZnPc singlet excited state with a comparably weak maximum at 840 nm and a lifetime of 3.1 ns in THF. This observation is in line with what was seen in the steady state emission experiments (*vide supra*). The ZnPc ground state bleaching at 610 and 680 nm develops within the same time span of 50 ps. Competitive with the energy transfer process the singlet excited state of ZnP decays via ISC resulting in the ZnP triplet excited state (~ 480 and 840 nm), which is stable over the window of the fs experimental setup (7.5 ns). Upon laser irradiation of **7** at 387 nm, all moieties are excited at the same time. Thus, a mixture of ZnP and ZnPc features is observed in the differential absorption spectra. To be more precise, maxima at 460, 580, and 630 nm correspond to the ZnP singlet excited state and decay within 50 ps. The ZnPc singlet excited state undergoes ISC to give the triplet manifold with its 500 and 840 nm absorption features within 1.7 ns. Transient bleaching is observed at 420, 560, and 610 nm as well as at 680 nm.
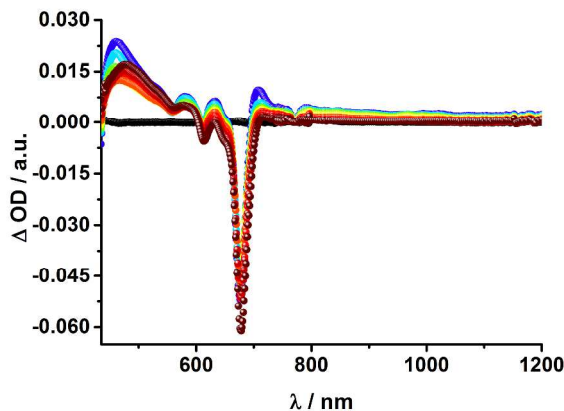
Fig. S13 Transient absorption spectrum (visible and near-infrared) registered upon femtosecond flash photolysis (387 nm, 200 nJ) of ZnP-ZnPc-(phen) thread **7** in tetrahydrofuran with time delays between 0 (black) and 7.5 ns (wine) at room temperature.

Excitation of rotaxane **6** at 420 nm yields the characteristic signatures of the ZnP singlet excited state at 450 nm that decay through energy transfer to give the rather weak singlet excited state of ZnPc with a lifetime of 1.0 ns, which is again in good agreement with the steady state experiments. In contrast to **7**, no triplet excited state features of ZnP could be observed. Instead the system decays exclusively via the ZnPc triplet excited state with its 480 nm fingerprint, which is stable on the 7.5 ns time scale. Additionally bleaching of ZnPc transients is observed at 610 and 680 nm. Upon exclusive excitation of ZnPc, in rotaxane **6** at 660 nm, the visible region is dominated by a broad peak maximizing at ~ 490 nm, which is stable over the time span of 7.5 ns and is assigned to the ZnPc triplet excited state. The ZnPc singlet excited state at 820 nm deactivates via ISC with 1.5 ns. At 680 nm, the ZnPc ground state bleaching is observed. At 387 nm all photoactive building blocks in rotaxane **6** were excited. Thus, the transient absorption spectra reveal a mixture of ZnP, ZnPc as well as $[Cu(phen)_2]^+$ features. As previously observed, the ZnP singlet excited state rapidly decays with 120 ps to give the ZnPc singlet excited state with a lifetime of 1.2 ns. The latter then decays via ISC to give the ZnPc triplet excited state, which is stable over the time scale of our fs setup. The MLCT absorption from $[Cu(phen)_2]^+$ exhibits a maximum at 910 nm, while in the visible part of the spectra it is masked by the ZnP and ZnPc transients. Since in **6** the ZnPc singlet state is significantly shorter lived than that seen for **7**, in line with time resolved fluorescence experiments, we conclude that the $[Cu(phen)_2]^+$ quenches the ZnPc fluorescence. No spectroscopic proof for charge separation is evident in the transient absorption spectra. Thus, only energy transfer to $[Cu(phen)_2]^+$ takes place in rotaxane **6**.
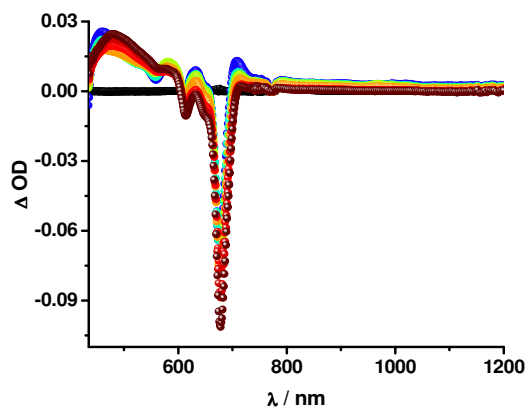
Fig. S 14 Transient absorption spectrum (visible and near-infrared) registered upon femtosecond flash photolysis (387 nm, 200 nJ) of ZnP-ZnPc-[Cu(phen)$_2$] rotaxane 6 in THF with time delays between 0 (black) and 7500 (wine) ps at room temperature.

5. Experimental Section

5.1. General Information and Materials

NMR spectra were obtained on either a Bruker AVANCE 400 (400 MHz) or an AVANCE 800 (800 MHz) spectrometer using deuterated solvents as the lock. The spectra were collected at $25^{o}C$ unless otherwise noted and chemical shifts (δ, ppm) were referenced to residual solvent peak (^1H, $CDCl_3$ at 7.26 ppm; ^{13}C at 77.2 ppm). In the assignments, the chemical shift (in ppm) is given first, followed, in brackets, by multiplicity (s, singlet; d, doublet; t, triplet; q, quadruplet, m, multiplet; br, broad), the value of the coupling constants in Hz if applicable, the number of protons implied and finally the assignment. In the ^1H NMR assignment (δ), H_o and H_m refer to the hydrogen atoms at the *ortho* and *meta* positions, respectively, of the phenyl ring attached to the phenanthroline ring system, whose hydrogen atoms are numbered $H_{3,8}$, $H_{4,7}$, $H_{5,6}$, respectively. Ar is used as an abbreviation for aromatic ring. Mass spectra were obtained on an Agilent 1100 Series Capillary LCMSD Trap XCT Spectrometer in positive or negative-ion mode and ThermoFinnigan PolarisQ ion-trap GCMS Spectrometer. MALDI-TOF mass spectra were recorded in a Bruker OmniFLEX MALDI-TOF MS Spectrometer. This instrument was operated at an accelerating potential of 20 kV in linear mode. The mass spectra represent an average over 128 consecutive laser shots. Mentioned *m/z* values correspond to monoisotopic masses. The compound solutions (10^{-3} mol/L) were prepared in THF. Matrix compound was purchased from Aldrich and used without further purification. The matrix, α-cyano-4-hydroxy-cinnamic acid (CCA), was dissolved (10 g/L) in a solvent mixture composed of H_2O/CH_3CN/TFA (25/75/1, v/v). Two microliters of compound solution was mixed with 10 μL of matrix solution. The final solution was deposited onto the sample target and allowed to dry in air. All chemicals were purchased from Sigma-Aldrich, Alfa Aesar and Acros Organics and used without further purification. For moisture sensitive reactions, solvents were freshly distilled. Methylene chloride (CH_2Cl_2) and acetonitrile (CH_3CN) were dried over calcium hydride while tetrahydrofuran (THF) was dried using sodium/benzophenone. Anhydrous dimethylformamide (DMF) was used as received. All syntheses were carried out using Schlenk techniques. Moisture sensitive liquids were transferred by cannula or syringe. The progress of the reactions was monitored by thin-layer chromatography (TLC) whenever possible. TLC was performed using precoated glass plates (Silica gel 60, 0.25 mm thickness) containing a 254 nm fluorescent indicator. Column chromatography was carried out using Merck Silica gel 60 (0.063-0.200 mm). Catenane model compounds 8 and 9 were prepared following the conditions reported in our previous work.[31] Compounds **10**[17], **11**[32], **12**[33], **13,**[1, 34,] **16**[8, 9, 32] **18**[1], **20**[33] and **22**[10] were synthesized following literature procedures.

5.2. Synthesis

Compound 14. In a three-necked round bottom flask, compound **13** (1.00 g, 1.60 mmol), and triethylamine (2 mL) were dissolved in 60 mL of dry CH_2Cl_2 under N_2 atmosphere with magnetic stirring. In an addition funnel, *p*-toluenesulfonyl chloride (*p*-TsCl) (0.304 g, 1.60 mmol) was dissolved in 20 mL of dry CH_2Cl_2. The round bottom flask was cooled to 0^oC and the *p*-TsCl solution was added dropwise (over 30 min) under N_2 atmosphere with magnetic stirring. After addition, the reaction mixture was kept at 0^oC for 4 h and then allowed to warm to rt and stirred for 12 h. The reaction was carefully quenched at $0\ ^oC$ by addition of 10% aqueous HCl. The organic phase was decanted, washed with water (3 x 50 mL), dried over Na_2SO_4, filtered through paper and concentrated under reduced pressure. Final purification was achieved by column chromatography (SiO_2) using CH_2Cl_2/MeOH as the eluent (gradient from 0 to 4%, v/v) to afford 14 as an orange oil (0.56 g, 45% yield). ^{1}H NMR ($CDCl_3$), δ ppm: 8.40 (d, *J* = 9.0 Hz*,* 4H, H$_o$); 8.27 (d, *J* = 9.0 Hz*,* 2H, H$_4$ and H$_7$); 8.09 (d, *J* = 9.0 Hz*,* 2H, H$_3$ and H$_8$); 7.77 (d, *J* = 9.0 Hz*,* 2H, *ortho* protons at Ar-OTs); 7.74 (s, 2H, H$_5$ and H$_6$); 7.34 (d, *J* = 9.0 Hz*,* 2H, *meta* protons at Ar-OTs); 7.12 (d, *J* = 9.0 Hz*,* 4H, H$_m$); 4.25–3.50 (set of signals, 24H, O–CH$_2$–CH$_2$–O); 2.39 (s, 3H, CH$_3$-Ar-OTs group). LC-MSD: m/z found 783.45 [M+H]$^+$, calculated 782.28 for $C_{43}H_{46}N_2O_{10}S$.

Compound 15. *Caution: Organic azides have been reported in literature as potential explosives. The authors suggest the use of standard PVC blast shield while handling organic azides.* Compound **14** (0.50 g, 0.64 mmol) and NaN$_3$ (0.125 g, 1.92 mmol) were dissolved in 15 mL of anhydrous DMF in a 100 mL Schlenk flask and the reaction mixture was heated at 80 ^oC for 12 h. The DMF was evaporated under reduced pressure. CH_2Cl_2 (50 mL) and H$_2$O (20 ml) was added, the organic phase was separated, washed with water (3 x 20 mL), dried over Na$_2$SO$_4$, filtered through paper and concentrated under reduced pressure. Final purification was achieved by flash chromatography (SiO_2) using CH_2Cl_2/MeOH (99:1, v/v) as the eluent, affording 15 as a light yellow solid (0.355 g, 85% yield). IR (KBr) v cm^{-1}: 2095 (N=N stretch).

Compound 17. Porphyrin carboxylic acid 16 (0.140 g, 0.132 mmol), **15** (0.086g, 0.132 mmol), EDC (0.051 g, 0.267 mmol), and DMAP (0.033g, 0.270 mmol) were place in in a 100 mL Schlenk flask and 25 mL of dry CH_2Cl_2 was added under N_2 atmosphere. The purple mixture was stirred at room temperature for 12 hours. The solution was washed with aqueous 10% HCl, then with water (3 x 10 mL), dried over Na$_2$SO$_4$, filtered through paper and concentrated under reduced pressure. Final purification was achieved by chromatography (SiO_2) using a gradient of CH_2Cl_2/MeOH (99:1, v/v) as the eluent to afford 17 as a purple solid (0.145 g, 65% yield). ^{1}H NMR ($CDCl_3$), δ ppm: 8.94 (s, 4H, H-pyrrolic); 8.86 (d, *J* = 6.5 Hz*,* 2H, H-pyrrolic); 8.72 (d, *J* = 6.5 Hz*,* 2H, H-pyrrolic); 8.35 (d, *J* = 9.0 Hz*,* 2H, H-*ortho* at Ar-COO); 8.26 (d, *J* = 8.9 Hz*,* 4H, H$_o$); 8.19 (d, *J* = 8.9 Hz*,* 2H, H$_{4,7}$); 8.01 (s, 6H, H-*ortho* at Ar-*t*Bu); 7.82 (s, 2H, H$_{5,6}$); 7.71 (s, 3H, H-*para* at Ar-*t*Bu); 7.56 and 7.51(d, *J* = 8.9 Hz*,* 2H, H$_{3,8}$); 7.12 (d, *J* = 9.0 Hz, 2H, H-*meta* at Ar-COO); 7.03 (d, *J* = 8.9 Hz*,* 2H, H$_m$); 6.96 (d, *J* = 8.9 Hz*,* 2H, H$_{m'}$); 4.60-3.90 (set of signals totalizing

24H, O–CH$_2$–CH$_2$–O); 1.45 (s, 54H, *t*-Bu). MALDI-TOF: m/z found 1692.99 [M+H]$^+$, calculated 1692.14 for C$_{105}$H$_{113}$N$_9$O$_8$Zn. IR (KBr) v cm^{-1}: 2091 (N=N stretch).

General Procedure for the Synthesis of Rotaxanes. In the reaction flask, the suitable phen-macrocycle deriva-tive (1.0 equiv.) and [Cu(CH$_3$CN)$_4$][PF$_6$] (1.0 equiv.) were dissolved in 1 mL of a mixture of CH$_2$Cl$_2$/CH$_3$CN (7:3, v/v) and the solution was stirred at room temperature under nitrogen atmosphere for 30 minutes. The appropriate phen-thread derivative (1.0 equiv.) was added as a solid and the reaction mixture was stirred at room tempera-ture under nitrogen atmosphere for 12 h. TLC showed quantitative formation of the pseudo-rotaxane precur-sors. The solvents were evaporated under reduced pressure and the remaining solid was dissolved in 4 mL of CH$_2$Cl$_2$ under nitrogen atmosphere. The suitable alkynyl derivative (2.5 equiv.) was added to the reaction flask as a solid. Meanwhile, in a second flask, CuI (2.0 equiv.), sodium ascorbate (8.0 equiv.) and sulfonated bathophe-nanthroline (4.0 equiv.) were dissolved in 2 mL of degassed H$_2$O/ethanol mixture (1:1, v/v). The resulting pink suspension was heated at reflux for 2 min and cooled back to rt. The resulting dark red solution was transferred to the reaction flask by syringe along with 1,8-diazabicycloundec-7-ene (DBU) (2.0 equiv.). The reaction mixture was stirred at room temperature under nitrogen atmosphere for 12 h. The crude mixture was neutralized by adding 10% HCl aqueous solution and extracted with CH$_2$Cl$_2$ (3 x 15 mL). The organic phase was washed with water (3 x 15 mL), concentrated to a volume of 5 mL and then stirred for 3 h with a saturated MeOH solution of KPF$_6$ (10 mL) to effect the anion exchange. The solvents were evaporated under reduced pressure, the remain-ing insoluble solid was extracted with CH$_2$Cl$_2$ (3 x 50 mL) and filtered through paper. The solvent was evaporated under reduced pressure and the crude product was purified by column chromatography (SiO$_2$) using appropriate CH$_2$Cl$_2$/CH$_3$OH mixture for each case as eluent. The excess alkynyl derivative was eluted first, followed by the corresponding thread compound, whose isolation indicates that some unthreading occurred during rotaxane assembly. The target rotaxane was the third eluted product from the column.

Rotaxane 1. This compound was prepared from macrocycle **18** (0.015 g, 10.6 µmol), thread **17** (0.018 g, 10.6 µmol) and commercially available alkynylferrocene (0.006 g, 26.5 µmol) following the general procedure for ro-taxanes synthesis. Final purification was achieved by column chromatography (SiO$_2$) using a gradient of CH$_2$Cl$_2$/CH$_3$OH (98:2, v/v) to yield the target compound as a dark red solid (0.034 g, 90% yield). MALDI-TOF: m/z found 3379.04 [M − PF$_6$]$^+$, calculated 3379.35 for C$_{216}$H$_{161}$N$_{11}$O$_{18}$CuFeZn.

Rotaxane 2. This compound was prepared from macrocycle **18** (0.015 g, 10.6 µmol), thread 17 (0.018 g, 10.6 µmol) and phthalocyanine **20** (0.020 g, 26.5 µmol) following the general procedure for rotaxanes synthesis. Final purification was achieved by column chromatography (SiO$_2$) using a gradient of CH$_2$Cl$_2$/CH$_3$OH (98:2, v/v) to yield the target compound as a deep blue solid (0.031 g, 72% yield). MALDI-TOF: m/z found 3939.90 [M − PF$_6$]$^+$, calcu-lated 3939.25 for C$_{250}$H$_{191}$N$_{19}$O$_{18}$CuZn$_2$.

Rotaxane 3. This compound was prepared from macrocycle **18** (0.015 g, 10.6 µmol), thread **22** (0.009 g, 10.6 µmol) and phthalocyanine **20** (0.020 g, 26.5 µmol) following the general procedure for rotaxanes synthesis. Final purification was achieved by column chromatography (SiO$_2$) using a gradient of CH$_2$Cl$_2$/CH$_3$OH (97:3, v/v) to yield the target compound as a green solid (0.028 g, 81% yield). MALDI-TOF: m/z found 3110.99 [M − PF$_6$]$^+$, calculated 3110.98 for C$_{192}$H$_{125}$N$_{15}$O$_{18}$CuFeZn.

Rotaxane 4. This compound was prepared from pentaethyleneglycol phen-macrocycle[35] (0.006 g, 10.6 µmol), thread **17** (0.018 g, 10.6 µmol) and commercially available alkynylferrocene (0.006 g, 26.5 µmol) following the general procedure for rotaxanes synthesis. Final purification was achieved by column chromatography (SiO$_2$) using a gradient of CH$_2$Cl$_2$/CH$_3$OH (98:2, v/v) to yield the target compound as a red solid (0.025 g, 88% yield). MALDI-TOF: m/z found 2532.22 [M − PF$_6$]$^+$, calculated 2531.72 for C$_{151}$H$_{157}$N$_{11}$O$_{14}$CuFeZn.

Rotaxane 6. This compound was prepared from pentaethyleneglycol phen-macrocycle[35] (0.006 g, 10.6 µmol), thread **17** (0.018 g, 10.6 µmol) and phthalocyanine 20 (0.020 g, 26.5 µmol) following the general procedure for rotaxanes synthesis. Final purification was achieved by column chromatography (SiO$_2$) using a gradient of CH$_2$Cl$_2$/CH$_3$OH (97:3, v/v) to yield the target compound as a blue solid (0.025 g, 88% yield). MALDI-TOF: m/z found 3091.82 [M − PF$_6$]$^+$, calculated 3091.24 for C$_{185}$H$_{187}$N$_{19}$O$_{14}$CuZn$_2$.

Compound 5. This thread model compound was isolated (red solid) as a byproduct from the synthesis of rotaxane **4** (0.002 g, 9% yield). To remove any copper contamination from the phen coordinating sites, the isolated material was dissolved in 2 mL of CH$_2$Cl$_2$/CH$_3$CN (1:1, v/v) mixture at room temperature and a saturated KCN aqueous solution (2 mL) was added. The resulting mixture was stirred at room temperature for 12 h. About 10 mL of CH$_2$Cl$_2$ was added to the crude mixture, the organic layer was decanted, copiously washed with water (5 x 10 mL), dried over Na$_2$SO$_4$, filtered through paper and concentrated under reduced pressure. Final purification was achieved by flash chromatography (SiO$_2$) using a gradient of CH$_2$Cl$_2$/MeOH (99:1, v/v) as the eluent to afford quantitatively the target compound as a red solid. Inductively-coupled plasma mass spectrometry (ICP-MS) analysis revealed a copper residual level of less than 250 ppm, which was a level acceptable for the spectroscopic investigation. MALDI-TOF: m/z found 1903.44 [M + H]$^+$, calculated 1902.22 for C$_{117}$H$_{123}$N$_9$O$_8$FeZn.

Compound 7. This thread model compound was isolated (blue solid) as a byproduct from the synthesis of rotaxane **6** (0.006 g, 22% yield). To remove any copper contamination from the phen coordinating sites, the isolated material was dissolved in 4 mL of CH$_2$Cl$_2$/CH$_3$CN (7:3, v/v) mixture at room temperature and a saturated KCN aqueous solution (4 mL) was added. The resulting mixture was stirred at room temperature for 12 h. About 10 mL of CH$_2$Cl$_2$ was added to the crude mixture, the organic layer was decanted, copiously washed with water (5 x 10 mL), dried over Na$_2$SO$_4$, filtered through paper and concentrated under reduced pressure. Final purification was achieved by flash chromatography (SiO$_2$) using a gradient of CH$_2$Cl$_2$/MeOH (99:1, v/v) as the eluent to afford

quantitatively the target compound as a blue solid. Inductively-coupled plasma mass spectrometry (ICP-MS) analysis revealed a copper residual level of less than 240 ppm, which was a level acceptable for the spectroscopic investigation. MALDI-TOF: m/z found 2479.95 $[M + H_2O]^+$, calculated 2461.74 for $C_{151}H_{153}N_{17}O_8Zn_2$.

5.3. Electrochemical and Photophysical Studies

All solvents used were purchased from commercial suppliers (spectroscopic grade; 99.5 %) and used without further purification. A single-compartment, three electrode cell configuration was used for the square wave voltammetry measurements, using a glassy carbon electrode (3 mm diameter) as a working electrode, a platinum wire as a counter and a silver wire as a reference electrode. All electrochemical measurements were performed with a METROHM FRA 2 µAutolab Type III potentiostat. For the photophysical characterization the samples were placed in fluorimetric cuvettes with different pathways and, when necessary, purged with molecular oxygen or argon. Steady-state UV-vis absorption spectroscopy was performed on a Lambda2 spectrometer (Perkin Elmer). Steady state fluorescence spectra were carried out at a FluoroMax3 spectrometer (Horiba) in the visible detection range and at a FluoroLog3 spectrometer (Horiba). Fluorescence lifetimes were determined by the time correlated single photon counting technique using a FlouroLog3 emission spectrometer (Horiba Jobin-Yvon) equipped with an R3809U-58 MCP (Hamamatsu) and an N-405LH laser diode (Horiba JobinYvon) exciting at 403 nm (300 ps fwhm) or a SuperK Extreme high power supercontinuum fiber laser EXW-12 (NKT) exciting at 420 nm (150 ps fwhm). Femtosecond transient absorption (TA) experiments were carried out with an amplified Ti:Sapphire laser system CPA-2110 fs laser (Clark MXR: output 775 nm, 1 kHz, and 150 fs pulse width) using a transient absorption pump/probe detection system (TAPPS Helios, Ultrafast Systems). The 420 nm excitation wavelength was generated with a noncolinear optical parametric amplifier (NOPA, Clark MXR). For the, excitation wavelength the energy of 150-200 nJ/ pulse was selected. Nanosecond transient absorption laser photolysis measurements were performed with the output from an optical parametric oscillator (OPO, Rainbow VIR, Opotek/Quantel, output: 425 and 670 nm, 5 mJ/pulse) pumped by the third harmonic (355 nm) of a Nd/YAG laser (Brilliant, Quantel). The optical detection was based on a pulsed (pulser MSP 05, Müller Elektronik-Optik) xenon lamp (XBO 450, Osram), a monochromator (Spectra Pro 2300i, Acton Research), a R928 photomultiplier tube (Hamamatsu Photonics), or a fast InGaAs photodiode (Nano 5, Coherent) with 300 MHz amplification, and a 1 GHz digital oscilloscope (WavePro7100, LeCroy). The experiments were performed on solutions in a 5x10 mm quartz glass cuvette.

6. Literature

1   J. D. Megiatto, Jr. D. I. Schuster, S. Abwandner, G. de Miguel and D. M. Guldi, *J. Am. Chem. Soc.*, 2010, **132**, 3847-3861.

2   J. D. Megiatto, Jr., R. Spencer and D. I. Schuster, *Org. Lett.*, 2009, **11**, 4152-4155.

3   J. D. Megiatto, Jr. and D. I. Schuster, *Chemistry*, 2009, **15**, 5444-5448.

4   F. Bitsch, C. O. Dietrich-Buchecker, A. K. Khemiss, J.-P. Sauvage and A. Van Dorsselaer, *J. Am. Chem. Soc.*, 1991, **113**, 4023-4025.

5   J. D. Megiatto and D. I. Schuster, *New J. Chem.*, 2010, **34**, 276.

6   E. J. Yoo, M. Ahlquist, S. H. Kim, I. Bae, V. V. Fokin, K. B. Sharpless and S. Chang, *Angew. Chem. Int. Ed. Engl.*, 2007, **46**, 1730-1733.

7   L. Flamigni, A. M. Talarico, J. C. Chambron, V. Heitz, M. Linke, N. Fujita and J.-P. Sauvage, *Chemistry*, 2004, **10**, 2689-2699.

8   K. Li, P. J. Bracher, D. M. Guldi, M. A. Herranz, L. Echegoyen and D. I. Schuster, *J. Am. Chem. Soc.*, 2004, **126**, 9156-9157.

9   K. Li, D. I. Schuster, D. M. Guldi, M. A. Herranz and L. Echegoyen, *J. Am. Chem. Soc.*, 2004, **126**, 3388-3389.

10   J. D. Megiatto, Jr., K. Li, D. I. Schuster, A. Palkar, M. A. Herranz, L. Echegoyen, S. Abwandner, G. Miguel and D. M. Guldi, *J. Phys. Chem. B*, 2010, **114**, 14408-14419.

11   J. D. Megiatto, Jr., D. I. Schuster, G. d. Miguel, S. Wolfrum and D. M. Guldi, *Chem. Mater.*, 2012, **24**, 2472-2485.

12   D. I. Schuster, K. Li, D. M. Guldi and J. Ramey, *Org. Lett.*, 2004, **6**, 1919-1922.

13   J. D. Megiatto Jr., R. Spencer and D. I. Schuster, *J. Mater. Chem.*, 2011, **21**, 1544.

14   C. Ornelas, J. Ruiz Aranzaes, E. Cloutet, S. Alves and D. Astruc, *Angew. Chem. Int. Ed. Engl.*, 2007, **46**, 872-877.

15   C. O. Dietrich-Buchecker and J.-P. Sauvage, *Chem. Rev.*, 1987, **87**, 795-810.

16   L. Echegoyen and L. E. Echegoyen, *Acc. Chem. Res.*, 1998, **31**, 593-601.

17   A. Hirsch and M. Brettreich, *Fullerenes: Chemistry and Reactions*, Wiley-VCH, Weinheim, 2005

18   S. Kirner, M. Sekita and D. M. Guldi, *Adv. Mater.*, 2014, **26**, 1482-1493.

19   S. V. Kirner, D. M. Guldi, J. D. Megiatto, Jr. and D. I. Schuster, *Nanoscale*, 2015, **7**, 1145-1160.

20   N. Armaroli, M. A. J. Rodgers, P. Ceroni, V. Balzani, C. O. Dietrich-Buchecker, J.-M. Kern, A. Bailal and J.-P. Sauvage, *Chem. Phys. Lett.*, 1995, **241**, 555-558.

21   T. Gunaratne, M. A. J. Rodgers, D. Felder, J.-F. Nierengarten, G. Accorsi and N. Armaroli, *Chem. Commun.*, 2003, 3010.

22   T. Kato, T. Kodama, T. Shida, T. Nakagawa, Y. Matsui, S. Suzuki, H. Shiromaru, K. Yamauchi and Y. Achiba, *Chem. Phys. Lett.*, 1991, **180**, 446-450.

23   Y. Rio, W. Seitz, A. Gouloumis, P. Vazquez, J. L. Sessler, D. M. Guldi and T. Torres, *Chemistry*, 2010, **16**, 1929-1940.

24   A. M. V. M. Pereira, A. R. M. Soares, A. Hausmann, M. G. P. M. S. Neves, A. C. Tomé, A. M. S. Silva, J. A. S. Cavaleiro, D. M. Guldi and T. Torres, *Phys. Chem. Chem. Phys.*, 2011, **13**, 11858.

25   C. Luo, D. M. Guldi, H. Imahori, K. Tamaki and Y. Sakata, *J. Am. Chem. Soc.*, 2000, **122**, 6535-6551.

26   A. Hausmann, A. R. Soares, M. V. Martinez-Diaz, M. G. Neves, A. C. Tome, J. A. Cavaleiro, T. Torres and D. M. Guldi, *Photochem Photobiol Sci*, 2010, **9**, 1027-1032.

27   M. Quintiliani, A. Kahnt, T. Wolfle, W. Hieringer, P. Vazquez, A. Gorling, D. M. Guldi and T. Torres, *Chemistry*, 2008, **14**, 3765-3775.

28   W. Seitz, A. Kahnt, D. M. Guldi and T. Torres, *J. Porphyrins Phthalocyanines*, 2009, **13**, 1034-1039.

29   R. F. Enes, J. J. Cid, A. Hausmann, O. Trukhina, A. Gouloumis, P. Vazquez, J. A. Cavaleiro, A. C. Tome, D. M. Guldi and T. Torres, *Chemistry*, 2012, **18**, 1727-1736.

30   A. J. Jimenez, M. L. Marcos, A. Hausmann, M. S. Rodriguez-Morgade, D. M. Guldi and T. Torres, *Chemistry*, 2011, **17**, 14139-14146.

31   A. M. Pereira, A. Hausmann, A. R. Soares, J. P. Tome, O. Trukhina, M. Urbani, M. G. Neves, J. A. Cavaleiro, D. M. Guldi and T. Torres, *Chemistry*, 2012, **18**, 3210-3219.

32   J. S. Lindsey, *Acc. Chem. Res.*, 2010, **43**, 300-311.

33   E. M. Maya, P. Vázquez and T. Torres, *Chem. Eur. J.*, 1999, **5**, 2004-2013.

34   C. O. Dietrich-Buchecker and J.-P. Sauvage, *Tetrahedron*, 1990, **46**, 503-512.

35   C. O. Dietrich-Buchecker and J.-P. Sauvage, *J. Am. Chem. Soc.*, 1984, **106**, 3043-3045.

Journal Name

Multistep Energy and Electron Transfer Processes in Novel Rotaxane Donor–Acceptor Hybrids Generating Microsecond Lived Charge Separated States

Sabrina V. Kirner, [a] Christian Henkel[a], Dirk M. Guldi, *[a] Jackson D. Megiatto, Jr. [b†] and David I. Schuster *[b]

Abstract: A new set of $[Cu(phen)_2]^+$ based rotaxanes, featuring [60]fullerene as an electron acceptor and a variety of electron donating moieties, namely zinc porphyrin (ZnP), zinc phthalocyanine (ZnPc) and ferrocene (Fc), has been synthesized and fully characterized with respect to their electrochemical and photophysical properties. The assembly of the rotaxanes has been achieved using a slight variation of our previously reported synthetic strategy that combines the Cu(I)-catalyzed azide-alkyne cycloaddition reaction (the "click" or CuAAC reaction) with Sauvage's metal-template protocol. To underline our results, complementary model rotaxanes and catenanes have been prepared using the same strategy and their electrochemistry and photo-induced processes investigated. Insights into excited state interactions have been afforded from steady state and time resolved emission spectroscopy as well as transient absorption spectroscopy. It has been found that photo-excitation of the present rotaxanes triggers a cascade of multi-step energy and electron transfer events that ultimately leads to remarkably long-lived charge separated states featuring one-electron reduced C_{60} radical anion ($C_{60}^{\bullet-}$) and either one-electron oxidized porphyrin ($ZnP^{\bullet+}$) or one-electron oxidized ferrocene ($Fc^{\bullet+}$) with lifetimes up to 61 microseconds. In addition, shorter-lived charge separated states involving one-electron oxidized copper complexes ($[Cu(phen)_2]^{2+}$ (τ < 100 ns), one-electron oxidized zinc phthalocyanine ($ZnPc^{\bullet+}$; τ = 380 – 560 ns), or one-electron oxidized zinc porphyrin (τ = 2.3 - 8.4 μs), and one electron reduced C_{60} have been identified as intermediates during the sequence. Detailed energy diagrams have been proposed for the rotaxanes to illustrate the sequence and rate constants of the photophysical events occurring with the mechanically-linked chromophores. This work pioneers the exploration of mechanically-linked systems as platforms to position more than three distinct chromophores, which are able to absorb light over a very wide range of the visible region, triggering a cascade of short-range energy and electron transfer processes to afford long-lived charge separated states.

[a.] Department of Chemistry and Pharmacy and Interdisciplinary Center for Molecular Materials, Friedrich-Alexander-Universität Erlangen-Nürnberg, D-91058 Erlangen, Germany.
[b.] Department of Chemistry, New York University, New York, NY 10003, USA.
† Present Address: Institute of Chemistry, University of Campinas, PO Box 6154, Campinas, SP, 13084-861, Brazil.

Introduction

In more than 25 years of fullerene research, C_{60} emerged as an excellent electron acceptor in electron transfer reactions, due to its unique properties. For instance, the rigid C_{60} cage can accept up to six electrons and has a very small reorganization energy in electron transfer reactions. Consequently, C_{60} has been utilized in photosynthetic reaction mimics, photovoltaics, and catalysis.[1] In order to guarantee efficient electron transfer, suitable electron donating moieties have to be chosen. In terms of photosynthetic reaction mimics, they have to fulfill the redox requirements imposed by the fullerene as well as to have the ability to efficiently harvest light. Both of these specifications are met by tetrapyrrolic macrocycles, such as porphyrins and phthalocyanines.

An interesting alternative to spatially arrange the chromophores is provided by mechanically-interlocked systems, such as catenanes and rotaxanes, decorated with electron donors and electron acceptors.[2-4] These photo-active interlocked platforms have allowed the systematic investigation of the effects of molecular topology on the thermodynamic and kinetic parameters of the electron and energy transfer processes in artificial photosynthetic models. This effort is motivated by the need to better understand the intricate roles that the protein environment plays in the photo-induced processes in natural photosynthesis.[5-10]

For example, we have shown, that catenanes[11] decorated with zinc porphyrin (ZnP) and C_{60} ultimately yield a charge separated state possessing $ZnP^{\bullet+}$ and $C_{60}^{\bullet-}$ radical ions with a lifetime roughly two times longer than the same charge separated state in the corresponding rotaxane.[12] This significant difference in lifetime reflects the distinct topology of the two interlocked systems. The catenane is conformationally rigid, while the rotaxane counterpart is not. Therefore, the former keep the ZnP and C_{60} moieties at longer and fixed distances, while the latter brings them closer to each other, a process that is driven by secondary interactions between the chromophores and allowed by the unclosed ring of the rotaxane.[11-19]

One of the well-established synthetic protocols to assemble rotaxanes and catenanes is Sauvage's Cu(I)-templated synthesis.[20-24] In this synthetic strategy, two 1,10-phenanthroline moieties (phen) become orthogonally arranged as a result of their tetrahedral coordination to the Cu(I) template ion, which creates the cross-over points needed for the formation of the mechanical bond. In the case of artificial photosynthetic models, the Cu(I) template synthesis ensures an additional benefit, namely the presence of an additional photoactive unit, the $[Cu(phen)_2]^+$ complex. It has been shown by us[12, 25] and others[26, 27] that the resulting $[Cu(phen)_2]^+$ complex facilitates the electronic communication between appended electron donors and electron acceptors on rotaxanes and catenanes upon photoexcitation.

The present work reports that a minor variation of this strategy has allowed the incorporation of porphyrin, phthalocyanine, and ferrocene electron donors as stoppering groups of $[Cu(phen)_2]^+$-

C_{60} based rotaxanes to afford a new family of multi-chromophoric interlocked structures (Fig. 1) that are able to undergo a cascade of energy and electron transfer reactions to yield charge separated states with remarkable long lifetimes. Furthermore, a complete set of model rotaxanes and catenanes lacking the electron donors, the C_{60} or both, were prepared using our synthetic protocol and probed as reference systems (Fig. 2). A complete and systematic investigation of the new interlocked compounds by electrochemistry, UV-Vis absorption, steady state, and time resolved emission spectroscopies as well as transient absorption spectroscopy in the femtosecond and nanosecond time regime has allowed us to gather the rates of the energy and electron transfer, charge shift, and charge recombination processes occurring upon photo-excitation of the three $[Cu(phen)_2]^+$-C_{60} rotaxanes to elucidate their deactivation processes.
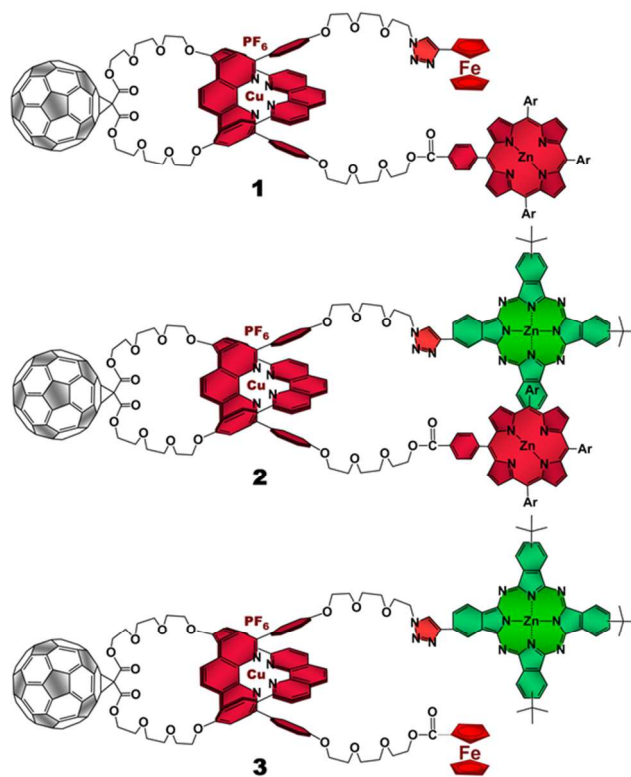

Fig. 1 $[Cu(phen)_2]^+$-C_{60} based rotaxanes (**1-3**) stoppered by three different combinations of electron donors investigated in the present work. Ar = 3,5-di-*tert*-butylphenyl.

Results and Discussion

1. Synthesis

The synthetic strategy used to prepare rotaxanes **1**-**3** is depicted in Scheme S1 (see SI). Briefly, one of the hydroxyl groups of compound **13**[11] is tosylated under classical conditions to yield **14**, which undergoes a nucleophilic substitution with sodium azide to afford **15**. The remaining hydroxyl group in **15** is esterified using 1-ethyl-3-(3-dimethyl-aminopropyl)carbodiimide (EDC) as coupling agent and dimethylaminopyridine (DMAP) as base following
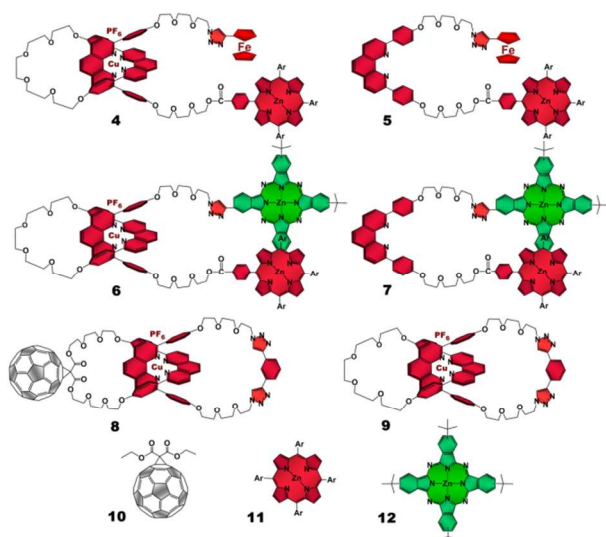
Fig. 2 Rotaxane and catenane models as well as reference compounds used to investigate the photophysical processes of the target rotaxanes.

the conditions reported in the experimental section (see SI) with either porphyrin **16**[28] or commercially available ferrocenecarboxylic acid **21** to produce the phen derivatives **17** and **22**, respectively. Threading of **17** or **22** through the C_{60}-based phen-macrocycle **18** using $[Cu(CH_3CN)_4]PF_6$ as the Cu(I) source in a mixture of dichloromethane/acetonitrile (7:3, v/v) at room temperature and under nitrogen atmosphere quantitatively yields pseudo-rotaxanes **19** and **23**, respectively, as revealed by TLC. Finally, pseudo-rotaxanes **19** or **23** and commercially available alkynyl ferrocene or phthalocyanine **20**[29] are submitted to our "click" protocol[11, 17, 30] to afford the target rotaxanes **1**, **2**, and **3**. Rotaxane and catenane model compounds were prepared following the same strategy from the appropriate building blocks.

2. Ground State Interactions – Absorption Spectra and Electrochemistry

The absorption spectra of rotaxanes **1**-**3** feature the typical absorption characteristics of the different building blocks (Fig. 3). In particular, rotaxane **1** exhibits broad absorption between 300 and 380 nm, corresponding to C_{60} and $[Cu(phen)_2]^+$. ZnP with its Soret and Q-bands reveals absorptions at 432, 561, and 602 nm. Compared to ZnTPP **11**, the ZnP absorption bands exhibit a red shift of around 3 nm. Ferrocene is spectroscopically invisible in the 300 to 700 nm range. Rotaxane **2** features additional absorption maxima corresponding to ZnPc, namely Soret and Q bands at 340, 616, and 685 nm. Here, the ZnP absorption bands are 2 nm red shifted compared to **1** or masked by the ZnPc absorption. Similarly, the absorption of C_{60} and $[Cu(phen)_2]^+$ is covered by that of ZnPc. The absorption spectrum of rotaxane **3** is dominated by the features corresponding to ZnPc, that is, maxima at 345, 613 and 679 nm, which are ~ 6 nm red shifted compared to reference **12**. Increased extinction coefficients in the Soret band region stem from C_{60} and $[Cu(phen)_2]^+$ absorptions.
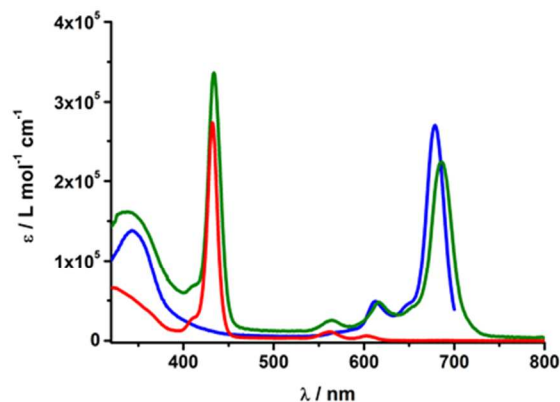
Fig. 3 UV/Vis absorption spectra of Fc-ZnP-$[Cu(phen)_2]$-C_{60} **1** (red), ZnP-ZnPc-$[Cu(phen)_2]$-C_{60} **2** (olive) and Fc-ZnPc-$[Cu(phen)_2]$-C_{60} **3** (blue) in PhCN.

Turning to electrochemistry (see Table S1) the redox chemistry of rotaxane **1** is best described as the superposition of catenane **8**, ZnTPP **11**, and ferrocene In particular, two one-electron reductions are seen within the electrochemical window of the solvent (dichloro-methane) at -1.09 and -1.45 V (all redox potentials are relative to Fc/Fc$^+$). Both are assigned to C_{60} centered reductions. As far as oxidation is concerned, three oxidations develop. As in rotaxane **4**, the first oxidation at +0.04 V is assigned to Fc, while the second, more intense oxidation at +0.24 V corresponds to a $[Cu(phen)_2]^+$-centered process as well as to the first ZnP oxidation. Likewise, the third oxidation at + 0.88 V correlates to the second ZnP oxidation.

Rotaxane **2** exhibits all the redox features seen for ZnTPP **11**, Zn^{t}Bu$_4$Pc **12**, and catenane **8**. To be more precise, two reductions at -1.13 and -1.54 V correspond to the reduction of C_{60}, while the oxidation of $[Cu(phen)_2]^+$ is observed at +0.13 V. As seen for **6** and **7**, the first ZnP and ZnPc oxidations cannot be clearly distinguished. A broader and more intense feature at +0.18 V is attributed to both. The second ZnP oxidation is observed at +0.83 V.

Finally, rotaxane **3** features two oxidations as well as two reductions within the electrochemical window. Here, the ferrocene oxidation is slightly shifted to less negative potentials, namely –0.05 V, possibly due to interactions with the other chromophores, while the second oxidation with about twice the intensity, is assigned to the one-electron oxidations of ZnPc and $[Cu(phen)_2]^+$. The reductive scan indicates two reductions of C_{60} at -1.10 and -1.55 V. Table S1 in the ESI sums up the redox potentials of compounds **1**-**12**.

3. Excited State Interactions - Fluorescence

Table S2 lists the fluorescence properties of the investigated rotaxanes as well as the corresponding references. The strongest fluorescent chromophore is ZnPc reference **12**. It has a fluorescence quantum yield of 0.3.[31, 32] Its fluorescence spectrum shows a maximum at 779 nm in THF and at 790 nm in PhCN - Fig. S5. ZnTPP **11**, with maxima at 602 and 655 nm in THF and 609 and

660 nm in PhCN, exhibits weaker fluorescence with a quantum yield of 0.04.

In contrast, the ZnP fluorescence in rotaxanes **1** and **4** is significantly quenched. Upon excitation at 420 nm, which coincides with the Soret band absorption maximum, a relatively weak ZnP fluorescence of 0.02 (Table S2) is observed for **1** and **4**, while in **5** the ZnP fluorescence is not quenched at all, which suggests energy and/or electron transfer from ZnP to $[Cu(phen)_2]^+$ and C_{60} occurs in **1** and **4**.

In rotaxane **2**, as well as in reference compounds **6** and **7**, the ZnPc fluorescence is quenched compared to **12** and the maximum emission is shifted to longer wavelengths. They show ZnPc fluorescence quantum yields between 0.07 and 0.13 in THF (Table S2) and between 0.09 and 0.24 in PhCN. The ZnP emission in rotaxanes **2** and **6** as well as in reference **7** is even more strongly quenched. Upon excitation into the porphyrin's Soret band at 420 nm only weak porphyrin fluorescence ranging from 0.004 to 0.008 (Table S2) is observed, which is partly overlaid by a strong fluorescence emission maximizing at ~ 690 nm with a shoulder at 760 nm (Fig. 4, top).
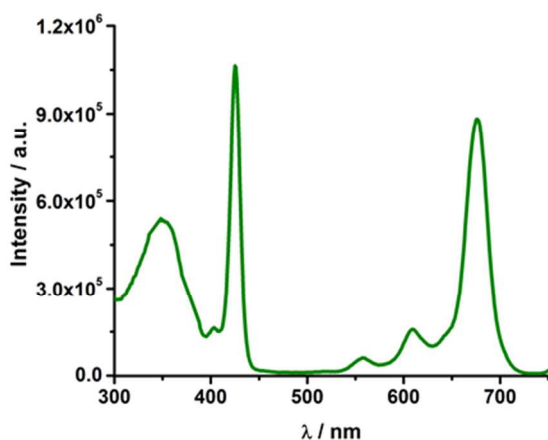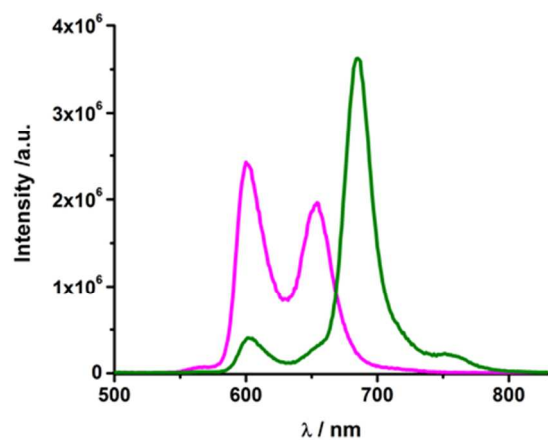

Fig. 4 Top: emission spectrum of rotaxane **2** (olive) and ZnTPP **11** (magenta) in THF upon excitation at 420 nm (OD=0.084); Bottom: excitation spectrum of rotaxane **2** in THF for emission at 760 nm.

Glancing at the excitation spectrum (Fig. 4 bottom) it becomes clear that this fluorescence originates from ZnPc, since the excitation spectrum corresponding to the 760 nm emission combines features of ZnP as well as of C_{60}. In contrast, the excitation spectrum of the 600 nm feature clearly proves that this fluorescence originates exclusively from ZnP. Thus, we postulate that an energy transfer from ZnP (2.06 eV) to the energetically lower lying ZnPc (1.8 eV) takes place. The quantum yield for this energy transfer was found to be 0.04 for rotaxane **2** in THF.

Rotaxane **3** exhibits 50 % quenched ZnPc fluorescence – Table S2. This quenching gives rise to the conclusion that energy and/or electron transfer from ZnPc to $[Cu(phen)_2]^+$ and to C_{60} takes place in these rotaxanes.

4. Excited State Interactions - Transient absorption spectroscopy To obtain information about the formation and decay processes of the excited states upon photoexcitation, transient absorption spectroscopy was carried out with rotaxanes **1**-**3** as well as references **4**-**12** (see SI) in THF using fs (387, 420 and 660 nm) as well as ns (355, 425 and 670 nm) laser excitation. Notably, we assume that the electron transfer processes are driven by through-bond rather than through-space interactions.

As time progresses, all of the aforementioned characteristics are replaced by a weak maximum at 1020 nm, which correlates with the fingerprint absorption of the one electron reduced form of C_{60}.[11,12,16,34] This is stable on the 7.5 ns timescale of our experimental setup. The signature of the one electron oxidized form of either $[Cu(phen)_2]^+$, ZnP, or Fc - as a complement to the one electron reduced form of C_{60} - are not discernible due to dominating ZnP singlet and triplet absorption features. The fact that the broad near-infrared transient is formed independently of the excitation wavelength leads us to conclude that energy transfer from ZnP to $[Cu(phen)_2]^+$ takes place. When comparing rotaxanes **1** and **4**, the ZnP fluorescence is quenched by 50 % relative to ZnTPP **11** in both cases. Thus, the lack of energy transfer to C_{60} is hypothesized.
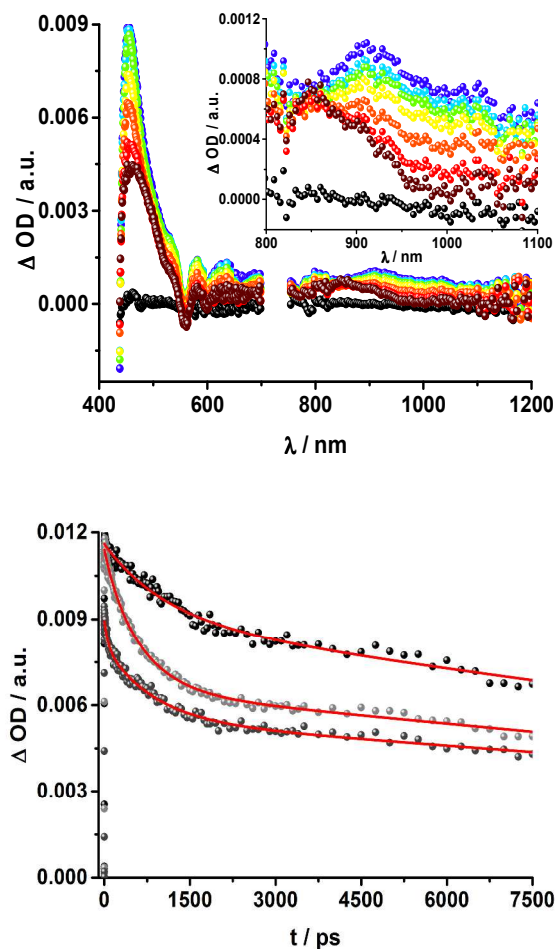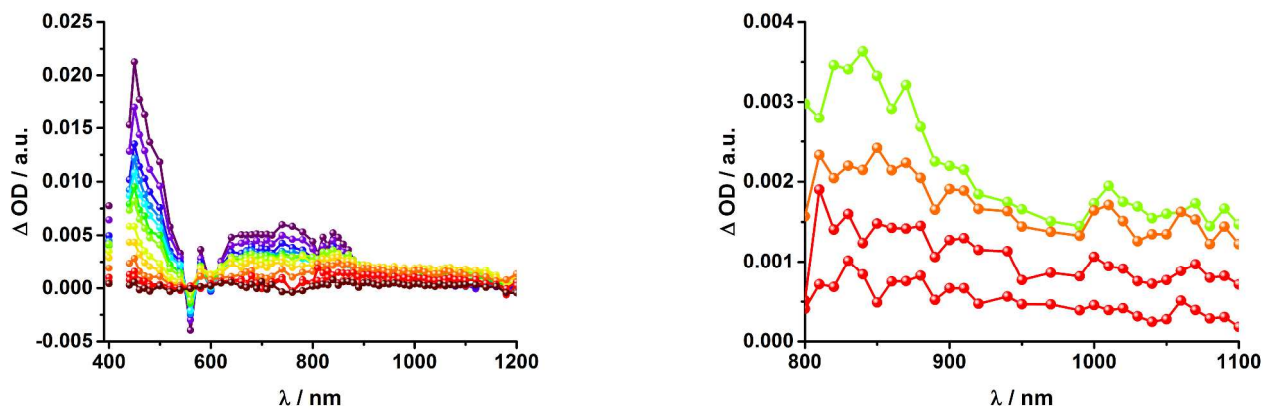
Fig. 5 Top: Transient absorption spectrum (visible and near-infrared) registered upon femtosecond flash photolysis (420 nm, 150 nJ) of Fc-ZnP-[Cu(phen)$_2$]$^+$-C$_{60}$ rotaxane **1** in tetrahydrofuran with time delays between 0 (black) and 7.5 ns (wine) at room temperature. Inset: zoom into the near infrared region. Bottom: time absorption profiles of **1** (dark grey), **4** (grey), and **5** (black) at 455 nm upon excitation with a 420 nm laser pulse, monitoring the decay of the ZnP singlet excited state.

Complementary transient absorption measurements on the ns timescale under aerobic conditions as well as in argon saturated THF shed light upon the excited state interactions in rotaxane **1**. Upon excitation at 425 nm, the differential absorption spectra are dominated by ZnP-centered features, namely the ZnP triplet

excited state with a broad absorption throughout the visible region and maxima at 460 and 840 nm (Fig. 6). In the absence of oxygen, a ZnP triplet excited state lifetime of 142 ± 12 μs was determined for rotaxane **1** in THF (Fig. 7). Notable is the fact that the triplet excited state of C$_{60}$ gives rise to a transient maximum at 740 nm, whose formation is masked by the dominating ZnP triplet excited state features.[11, 12] A closer look at the differential absorption changes reveals additional peaks, which are discernible at 680 and 1010 nm (Fig. 6). In line with previous reports, the latter is assigned to the one electron reduced form of C$_{60}$, while the former correlates with the one electron oxidized form of ZnP.[11, 14, 15, 18, 33, 35] From the corresponding extinction coefficients, that is, 0.82 x 10^4 M^{-1}cm^{-1} for the ZnP triplet excited state at 840 nm[36] and 1.5 x 10^4 M^{-1}cm^{-1} for the one electron reduced form of C$_{60}$,[37] we conclude that the major product is the former. However, exact values for the yields of charge separation could not be determined. Similarly, upon ns-excitation of rotaxane **1** a long-lived ZnP$^{•+}$/C$_{60}$$^{•-}$ charge separated state is formed in addition to the ZnP triplet excited state. Evidence for the transient formation of one electron oxidized ferrocene and/or [Cu(phen)$_2$]$^+$ is hampered by their very low extinction coefficients.[38-43] Interactions in terms of energy transfer are unlikely to happen but cannot be ruled out with certainty.

To dissect the different contributions in the transient absorption measurements on rotaxane **1**, that is, the ZnP$^{•+}$/C$_{60}$$^{•-}$ charge separated state, the ZnP triplet excited state, and the C$_{60}$ triplet excited state, the decay kinetics of the one electron oxidized form of ZnP at 680 nm and the one electron reduced form of C$_{60}$ at 1010 nm were analyzed in the presence or absence of oxygen. It is well known that oxygen impacts the triplet excited state lifetime of ZnP (Table S3).[44, 45] We find that the transient at 680 nm decays biexponentially (Fig. S7, left) with one lifetime that depends strongly on the O$_2$ concentration and another one that is nearly constant; 112 μs is the lifetime in the absence of O$_2$ and 110 ns under O$_2$ saturated conditions (Table S3), from which a bimolecular quenching rate constant of 1.0 x 10^9 M^{-1}s^{-1} is derived. The other component has a nearly constant lifetime of 2.3 ± 0.3 μs. The O$_2$-dependent lifetime must relate to the ZnP triplet excited state, whereas the component that shows only a weak O$_2$ dependence is assigned to the charge separated state involving the one electron oxidized form of ZnP. Note that the extinction

Fig. 6 Left: differential absorption spectra (visible and near infrared) registered upon nanosecond flash photolysis (425 nm, 5 mJ) of Fc-ZnP-[Cu(phen)$_2$]$^+$-C$_{60}$ rotaxane **1** under aerobic conditions in tetrahydrofuran with time delays between 200 ns (purple) and 15 μs (wine) at room temperature. Right: differential absorption spectra (near infrared) registered upon nanosecond flash photolysis (420 nm, 5 mJ) of Fc-ZnP-[Cu(phen)$_2$]$^+$-C$_{60}$ rotaxane **1** under aerobic conditions in tetrahydrofuran with time delays between 1 (green) and 5 μs (red) at room temperature.
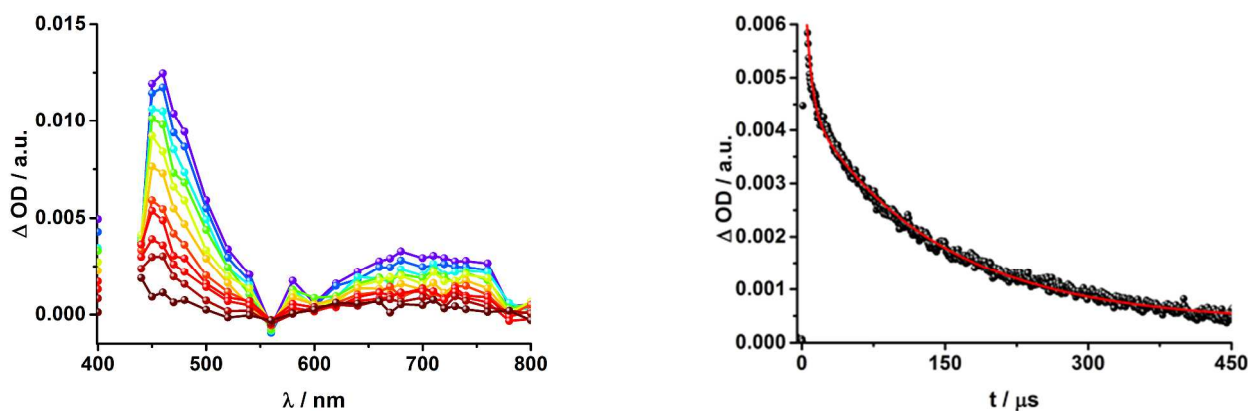

Fig. 7 Left: differential absorption spectra (visible) registered upon nanosecond flash photolysis (425 nm, 5 mJ) of Fc-ZnP-[Cu(phen)$_2$]$^+$-C$_{60}$ rotaxane **1** under argon atmosphere in tetrahydrofuran with time delays between 8 μs (purple) and 400 μs (wine) at room temperature. Right: Time absorption profile of the spectra on top at 460 nm, monitoring the decay of the ZnP triplet excited state.

coefficient of the one electron oxidized form of Fc is lower than that of ZnP with a value of 500 M^{-1} cm^{-1}.[15] In light of the afore-mentioned, we analyzed the decay of the one electron reduced form of C$_{60}$ - Fig. S7 - at 1010 nm. From tri-exponential fittings a short lifetime of 55 ± 8 ns as well as an intermediate and a long lifetime of 2.3 ± 0.4 and 61 ± 16 μs were derived. Only the intermediate and long lifetimes exhibit dependence on the concentration of O$_2$, yielding bimolecular rate constants of 1.0 x 10^7 and 1.7 x 10^5 M^{-1}s^{-1}, respectively. Considering that the short lifetime is comparable to that found for **8**[11,12,18,33] it is, in turn, assigned to Fc-ZnP-[Cu(phen)$_2$]$^{2+}$-C$_{60}$$^{\bullet-}$. The intermediate lifetime of the 1010 nm decay matches the 680 nm decay, which implies that it is the Fc-ZnP$^{\bullet+}$-[Cu(phen)$_2$]$^+$-C$_{60}$$^{\bullet-}$ charge separated state. Finally, the long lifetime is assigned to the Fc$^{\bullet+}$-ZnP-[Cu(phen)$_2$]$^+$-C$_{60}$$^{\bullet-}$ charge separated state, since it possesses the lowest energy (1.13 eV).

Fig. 8 schematically correlates the processes, which take place upon 425 nm excitation of rotaxane **1** with the corresponding energy levels calculated from spectroscopic and electrochemical data. Excitation of rotaxane **1** into the ZnP Soret band at 425 nm generates its singlet excited state with an energy level of 2.06 eV relative to the ground state. From these states, different deacti-vation pathways emerge. Firstly, a deactivation to the ground state via fluorescence occurs with a quantum yield of 2 %. Sec-ondly, intersystem crossing (ISC) yields the energetically lower-lying ZnP centered triplet excited state (1.50 eV), which subse-quently decays to the ground state. In competition, energy transfer from the ZnP singlet excited state to [Cu(phen)$_2$]$^+$ takes place. The aforementioned energy transduction to [Cu(phen)$_2$]$^+$ is followed by a rapid and unresolvable ISC to ^{3}MLCT*. From the latter, electron transfer generates the one electron reduced C$_{60}$ and the one electron oxidized [Cu(phen)$_2$]$^{2+}$ with an energy level at 1.31 eV above the ground state. Experimental confirmation for this electron transfer hypothesis comes from comparison between the *ns* transient absorption data for **1** with those ob-tained for catenane **8**. The lifetime of C$_{60}$$^{\bullet-}$ of 55 ns (k$_{CR}$ = 1.8 x

10^7 s^{-1}) in **1** resembles that found for catenane **8** (100 ns).[11, 12, 16, 33] Despite the fact that [Cu(phen)$_2$]$^{2+}$ cannot be identified in the differential absorption spectra, due to its low extinction coefficient, we are confident about the formation and existence of the Fc-ZnP-[Cu(phen)$_2$]$^{2+}$-C$_{60}^{\bullet-}$ charge separated state. From this intermediate state, a charge shift process occurs from [Cu(phen)$_2$]$^{2+}$ to ferrocene and/or to ZnP. On longer time scales, two additional lifetimes were derived for the one electron reduced C$_{60}$, one of which matches the lifetime of 2.3 μs (k_{CR} = 4.3 x 10^5 s^{-1}) found for the one electron oxidized ZnP at 680 nm. Accordingly, this lifetime is assigned to the Fc-ZnP$^{\bullet+}$-[Cu(phen)$_2$]$^{+}$-C$_{60}^{\bullet-}$ charge separated state, which is isoenergetic with the Fc-ZnP-[Cu(phen)$_2$]$^{2+}$-C$_{60}^{\bullet-}$
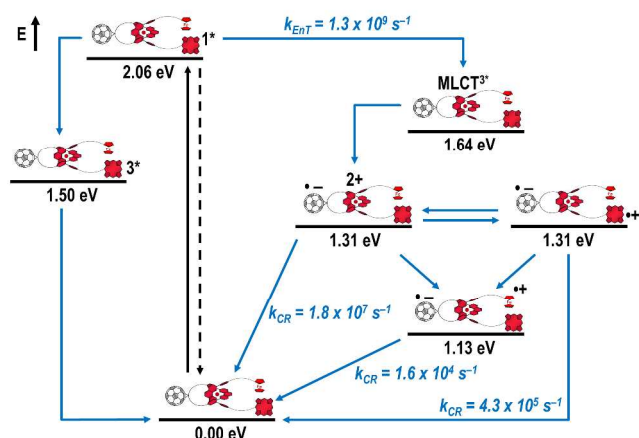

Fig. 8 Schematic energy level diagrams, proposed decay pathways and rate constants for Fc-ZnP-[Cu(phen)$_2$]$^{+}$-C$_{60}$ rotaxane **1** upon excitation at 425 nm. k_{EnT} = energy transfer rate; k_{CR} = charge recombination rate.

one, therefore favoring the interaction between these two states. The lifetime of 61 μs (k_{CR} = 1.6 x 10^4 s^{-1}) is attributed to the Fc$^{\bullet+}$-ZnP-[Cu(phen)$_2$]$^{+}$-C$_{60}^{\bullet-}$ charge separated state. This state is expected to be the thermodynamically most stable state at 1.13 eV relative to the ground state (Fig. 8). This stable state can be generated by two thermodynamically possible charge shift scenarios, that is, one evolving from Fc-ZnP-[Cu(phen)$_2$]$^{2+}$-C$_{60}^{\bullet-}$ and the other from Fc-ZnP$^{\bullet+}$-[Cu(phen)$_2$]$^{+}$-C$_{60}^{\bullet-}$. Considering the slow charge recombination in Fc$^{\bullet+}$-ZnP-[Cu(phen)$_2$]$^{+}$-C$_{60}^{\bullet-}$, with a rate constant of k_{CR} = 1.6 x 10^4 s^{-1}, it is concluded that charge recombination is located in the inverted region of the Marcus parabola.[46, 47]

Excitation of rotaxane **2** at 660 nm yields the ZnPc singlet excited state identified by the 825 nm signature absorption. The latter deactivates via ISC. This triplet excited state with its 490 nm marker is stable on the time scale of the experiment. Ground state bleaching is observed at 610 and 680 nm. Additionally, a new peak in the near infrared region at 1010 nm emerges, which is the fingerprint of the one electron reduced C$_{60}$. From this, we conclude that electron transfer takes place in rotaxane **2** in competition with ISC. Excitation into the ZnP Soret band of **2** at 420 nm results in population of the ZnP singlet excited state which

decays within 40 ps to give the analogous triplet excited state as well as the energetically lower lying ZnPc singlet excited state, as found for **6** and **7** (SI). Here, no clear signs for any transduction of excited state energy were found.

Upon excitation of rotaxane **2** at 387 nm, not just the ZnP and ZnPc transient features are observed in the differential absorption spectra, as seen upon 660 and 420 nm excitation, but also those of C$_{60}$ and [Cu(phen)$_2$]$^{+}$ (Fig. 9). In the visible region of the spectrum, the C$_{60}$ singlet excited state marker at 510 nm and ^{3}MLCT* marker at 600 nm are masked by the more intense ZnP and ZnPc transient absorptions. In the near-infrared region, a rather broad transient absorption is observed that corresponds to the triplet MLCT state. Additionally, two maxima are identified at 850 and 1020 nm in PhCN or 840 and 1020 nm in THF. The 1020 nm transients, the well-known fingerprint of the one electron reduced C$_{60}$, are stable over the 7.5 ns time scale of our experiment.[48, 49] The 840-850 nm transient corresponds to the ZnPc singlet excited state with a lifetime of 2.2 ns in PhCN and 1.6 ns in THF. Notably, mono-exponential fitting is not sufficient to describe the underlying transient decay. The 850 nm transient, which is stable over the 7.5 ns time scale, can be assigned to the one electron oxidized ZnPc.[50] Thus, we conclude that electron transfer from ZnPc to C$_{60}$ takes place. The possibility that ZnP is also involved in an electron transfer process cannot be ruled out, since its transient feature coincides with the ZnPc ground state bleaching. However, based on thermodynamics this pathway is very unlikely to happen.
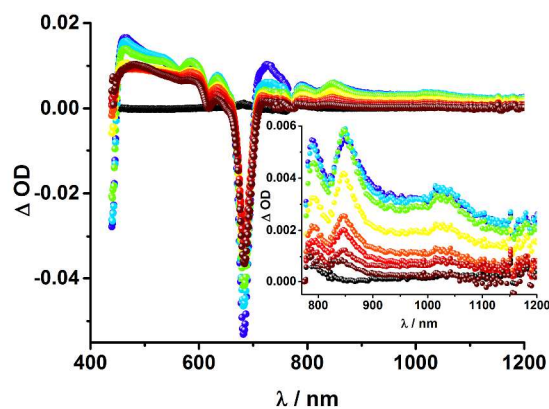
Fig. 9 Transient absorption spectrum (visible and near-infrared; Inlet: near infrared) registered upon femtosecond flash photolysis (387 nm, 200 nJ) of ZnP-ZnPc-Cu(phen)$_2$-C$_{60}$ rotaxane **2** in PhCN with time delays between 0 (black) and 7.5 ns (wine) at room temperature. Inset: zoom into the near infrared region.

In complementary ns-transient absorption experiments, rotaxane **2** was excited into the ZnP Soret band at 425 nm and into the ZnPc Q-band at 670 nm. Upon ZnPc excitation, the visible region of the differential absorption spectra is dominated by the broad ZnPc triplet excited state signature at 480 nm (Fig. 10, left). The latter is oxygen sensitive, with lifetimes of ~ 300 ns in the presence of oxygen and ~ 14 μs in the absence of oxygen. Signature
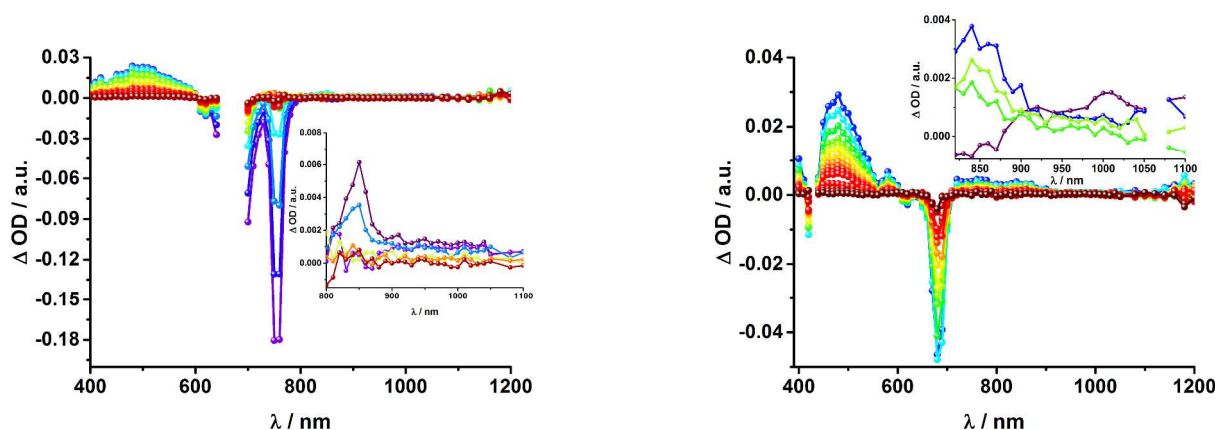
Fig. 10 Left: differential absorption spectra (visible and near infrared) registered upon nanosecond flash photolysis (670 nm, 5 mJ) of ZnP-ZnPc-[Cu(phen)$_2$]$^+$-C$_{60}$ rotaxane **2** under aerobic conditions in tetrahydronfuran with time delays between 90 ns (blue) and 1.0 μs (wine) at room temperature. Inset: zoom into the near infrared region with time delays between 65 ns (purple) and 1.0 μs (wine). Right: differential absorption spectra (visible and near infrared) registered upon nanosecond flash photolysis (425 nm, 5 mJ) of ZnP-ZnPc-[Cu(phen)$_2$]$^+$-C$_{60}$ rotaxane **2** under aerobic conditions in tetrahydrofuran with time delays between 120 ns (blue) and 4.0 μs (wine) at room temperature. Inset: zoom into the near infrared region with time delays between 23 ns (purple) and 400 ns (green).

absorption corresponding to C$_{60}$ triplet excited state and/or ^{3}MLCT* were not observed due to the intense ZnPc ground state bleaching between 650 and 750 nm. In the near-infrared region, two maxima are discernible at 850 and 1010 nm. The former is assigned to the one-electron oxidized ZnPc, which decays with a lifetime of ~ 520 ± 100 ns, while the latter is the one-electron reduced C$_{60}$ and exhibits two decay lifetimes, 64 ± 26 ns and 570 ± 110 ns. The shorter lifetime matches those found for reference **8**[11, 12, 16, 33] and the close charge separated states in rotaxane **1**. Thus, it is assigned to the [Cu(phen)$_2$]$^+$ centered charge separated state ZnP-ZnPc-[Cu(phen)$_2$]$^{2+}$-C$_{60}$$^{•-}$. The longer lifetime is in agreement with the ZnP-ZnPc$^{•+}$-[Cu(phen)$_2$]$^+$-C$_{60}$$^{•-}$ charge separated state. No indication of a charge shift to form ZnP$^{•+}$-ZnPc-[Cu(phen)$_2$]$^+$-C$_{60}$$^{•-}$ was seen upon 670 nm excitation.

When exciting into the ZnP Soret band at 425 nm, the transient absorption spectra are slightly different (Fig. 10, right). Here, the dominant features belong to those of ZnP with maxima at 480 and 840 nm. The biexponential decay of the 480 nm transients, gives lifetimes corresponding to the triplet excited state of ZnP (140 μs under Ar) as well as that of ZnPc (14 μs under Ar). Thus, it is reasonable to assume that upon excitation of ZnP two deactivation pathways occur; ISC to the triplet manifold and energy

transfer to ZnPc followed by ISC. This observation is also in agreement with the fs transient absorption data. In additional to the strongly oxygen dependent ZnPc triplet excited state lifetime, the decay at 840 nm yields a second component with a lifetime of 560 ± 100 ns. This lifetime correlates with that seen for the one-electron oxidized ZnPc, as seen upon 670 nm excitation. Furthermore, the decay of the one-electron reduced C$_{60}$ at ~1010 nm can be fit with three lifetimes, 63 ± 16 ns, 590 ± 150 ns, and 8.4 ± 1.0 μs (Fig. 11). Again, the shortest lifetime is assigned to ZnP-ZnPc-[Cu(phen)$_2$]$^{2+}$-C$_{60}$$^{•-}$. In contrast to the 670 nm excitation, here two different charge shifts seem to occur. Firstly, the ZnPc centered charge separated state ZnP-ZnPc$^{•+}$-[Cu(phen)$_2$]$^+$-C$_{60}$$^{•-}$ with a lifetime of 560 ± 120 ns (from 840 and 1010 nm decays) is formed. Secondly, the longer lived ZnP centered charge separated state ZnP$^{•+}$-ZnPc-[Cu(phen)$_2$]$^+$-C$_{60}$$^{•-}$ with a lifetime of 8.4 μs is generated. The corresponding cation again cannot be identified, since it coincides with the ZnPc ground state bleaching in the 680 nm region. Overall, these results are in agreement with the transient lifetimes found for rotaxane **1**. A schematic energy level diagram of the photoinduced processes in rotaxane **2** is shown in Fig. 12, including energy levels calculated from electrochemical and spectroscopic data. Two different excitation
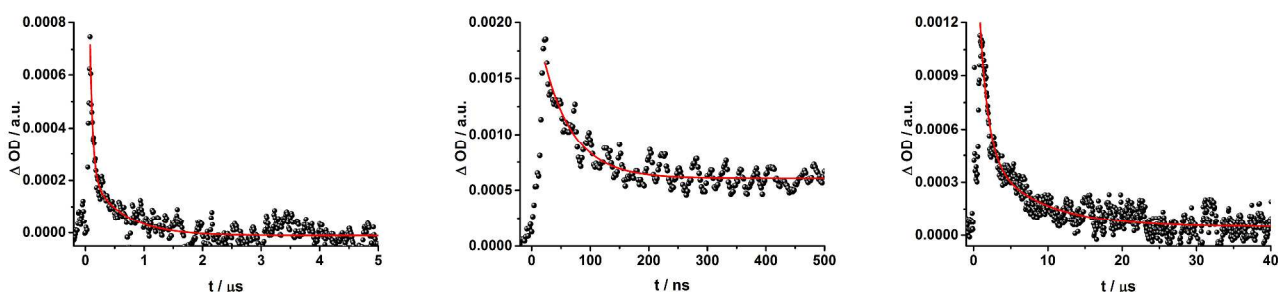
Fig. 11 Time absorption profiles at 10-10 nm of ZnP-ZnPc-[Cu(phen)$_2$]$^+$-C$_{60}$ rotaxane **2** in tetrahydrofuran at room temperature under aerobic conditions upon excitation at 670 nm (left) and 425 nm (center and right), monitoring the charge recombination.
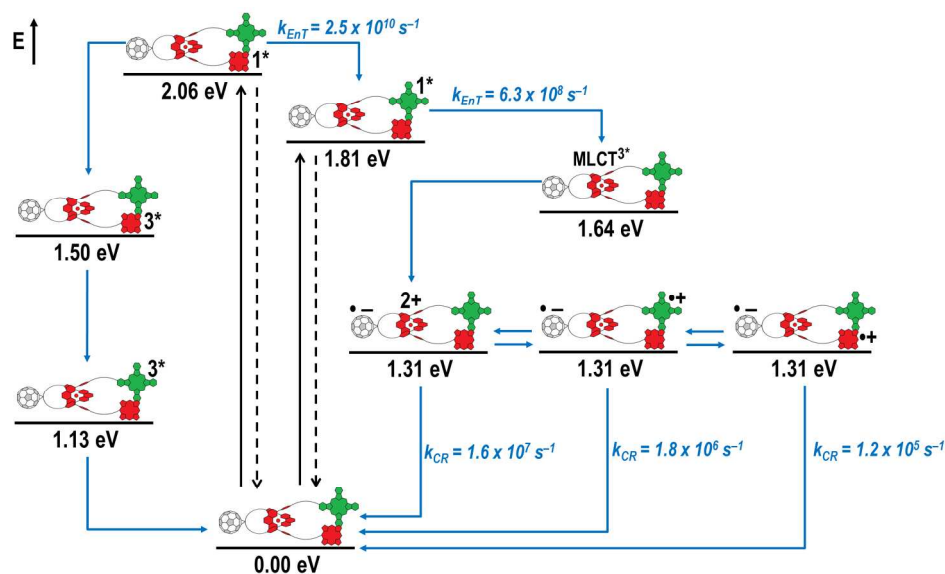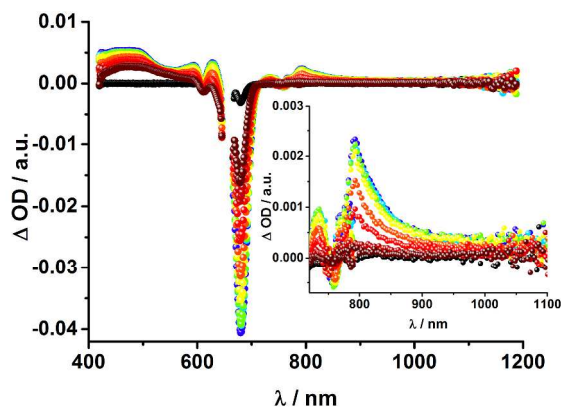
Fig. 12 Schematic energy level diagrams, proposed decay pathways and rate constants for ZnP-ZnPc-[Cu(phen)$_2$]$^+$-C$_{60}$ rotaxane **2** upon excitation at 425 nm (purple and black arrows) and 670 nm (red and black arrows). k_{EnT} = energy transfer rate k_{CR} = charge recombination rate.

routes are feasible, which result in slightly different deactivation processes. When exciting ZnPc at 670 nm, its singlet excited state is immediately formed, with an energy level of 1.81 eV relative to the ground state. Deactivation via fluorescence (12 %) as well as via ISC takes place. In parallel, energy transfer from the ZnPc singlet excited state to [Cu(phen)$_2$]$^+$ occurs, which is verified by ~ 80 % quenching of the ZnPc fluorescence (Table S2). Next, the ^{1}*MLCT undergoes rapid ISC to give ^{3}MLCT* (1.64 eV). By analogy to **1**, the ^{3}MLCT* decays through electron transfer to yield the charge separated state ZnP-ZnPc-[Cu(phen)$_2$]$^{2+}$-C$_{60}$$^{\bullet-}$. The rate constant for the charge recombination of ZnP-ZnPc-[Cu(phen)$_2$]$^{2+}$-C$_{60}$$^{\bullet-}$ is 1.6 x 10^7 s^{-1} (63 ns), in the same range as that observed for **8**^{11,12,18,33} and **1**. A charge shift from the oxidized [Cu(phen)$_2$]$^{2+}$ to ZnPc yields the charge separated state ZnP-ZnPc$^{\bullet+}$-[Cu(phen)$_2$]$^{2+}$-C$_{60}$$^{\bullet-}$, whose formation is corroborated by the observation of the same lifetimes (560 ns, k$_{CR}$ = 1.8x10^6 s^{-1}) for the one electron oxidized ZnPc and the one electron reduced C$_{60}$. No proof for the formation of the ZnP centered charge separated state was found upon 670 nm excitation. However, when exciting rotaxane **2** at 425 nm, the ZnP singlet excited state (2.06 eV) is formed and additional decay pathways emerge. On one hand, the ZnP triplet excited state (~ 1.5 eV) is generated via ISC, which decays back to the ground state. On the other hand, energy transfer to the energetically lower lying ^{1}*ZnPc (1.81 eV) takes place, which has been observed by fluorescence as well as excitation spectra (Fig. 4 and Table S2). From this point on, the same processes occurring upon excitation at 670 nm take place. However, when taking a closer look at the one electron reduced C$_{60}$ decay at 1010 nm, a third much longer lifetime of 8.4 µs (k$_{CR}$ = 1.2x10^5 s^{-1}) was identified. Consequently, we conclude that upon excitation of rotaxane **2** at 425 nm, a second charge shift from ZnP-ZnPc$^{\bullet+}$-[Cu(phen)$_2$]$^{2+}$-C$_{60}$$^{\bullet-}$ takes place to form the ZnP centered charge separated state ZnP$^{\bullet+}$-
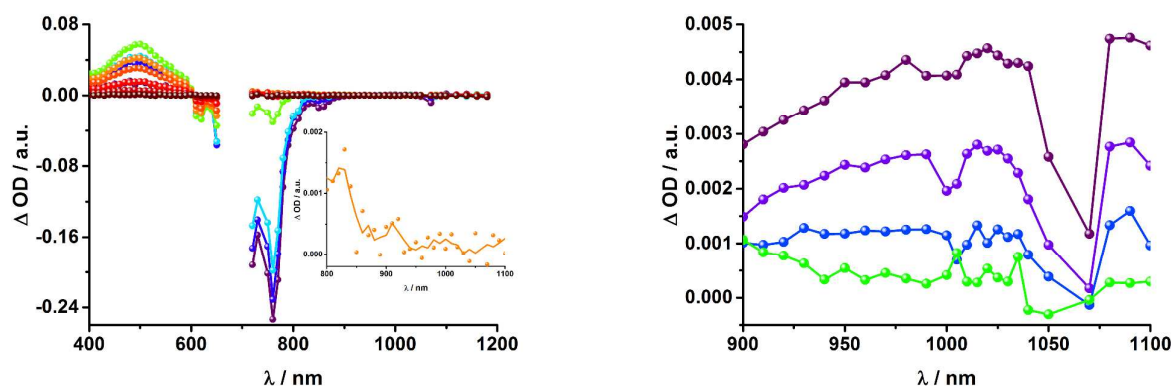
ZnPc-[Cu(phen)$_2$]$^{2+}$-C$_{60}$$^{\bullet-}$. Considering the energy of the three different charge separated states relative to the ground state, it must be noted that they exhibit approximately the same energy level (1.31 eV), since the oxidation potentials of [Cu(phen)$_2$]$^+$, ZnP, and ZnPc do not differ appreciably.

Finally, rotaxane **3** was probed with our fs transient absorption setup. The 660 nm fs-excitation exclusively excites ZnPc. Immediately after the laser pulse the ZnPc singlet excited state arises with a maximum at 790 nm and a lifetime of 1.9 ns in THF (800 nm, 1.9 ns in PhCN) (Fig. 13). The singlet excited state decays via intersystem crossing (ISC) to the energetically lower lying triplet excited state (~ 480 nm), which is stable over the time scale of our experimental setup (7.5 ns). Additionally, ground state bleaching leads to minima at 610 and 680 nm in THF and 615 and 690 nm in PhCN. No clear assignment of transients corresponding to C$_{60}$, [Cu(phen)$_2$]$^+$, or any charge separated state could be made in the fs transient absorption experiments, due to their low extinction coefficients and the relatively low energy of the laser excitation (150 nJ). Weak, but broad transient absorptions in the near infrared region (Fig. 13, inset) allows us to conclude that energy transfer occurs to yield the ^{3}MLCT* state.
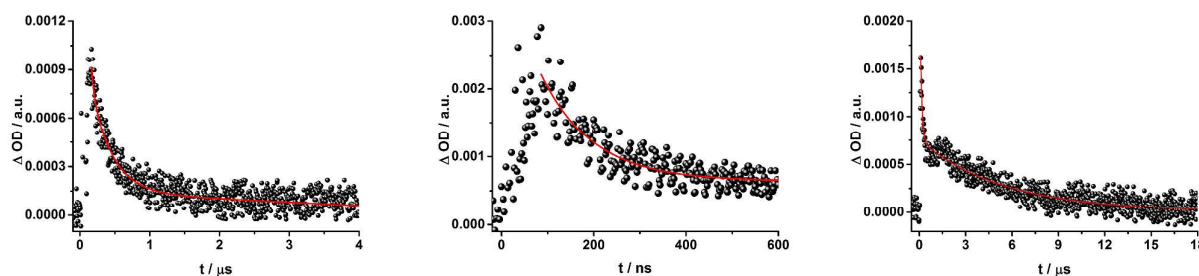
Fig. 13 Transient absorption spectrum (visible and near-infrared) registered upon femtosecond flash photolysis (660 nm, 150 nJ) of Fc-ZnPc-$[Cu(phen)_2]^+$-C_{60} rotaxane **3** in tetrahydrofuran with time delays between 0 (black) and 5.8 ns (wine) at room temperature. Inset: zoom into the near infrared region.

To gain further insight into the charge transfer dynamics, we turned to longer time scales. Upon ns-excitation (note that in the ns experiment the laser energy is significantly higher than in the fs experiments) of the ZnPc Q-band at 670 nm, the visible region of the differential absorption spectra is dominated by the triplet excited state signature of ZnPc with its maximum at 500 nm accompanied by ground state bleaching at 610 and 690 nm (Fig. 14, left).[51-57] In the near-infrared region (Fig. 14), the broad ^{3}MLCT* absorption (~900-1000 nm) is observed. Additionally, two peaks are discernible at 830 and 1020 nm. The former is assigned to the one-electron oxidized ZnPc, which decays mono-exponentially with a lifetime of 380 ± 60 ns (Fig. 15, left). The peak at 1020 nm corresponds to the one-electron reduced C_{60} and it is best fit with three exponentials, as seen earlier for rotaxanes **1** and **2** (Fig. 15, center and right). The shortest lifetime of 88 ± 9 ns resembles that found in catenane **8**[11,12,18,33] and is ascribed to the $[Cu(phen)_2]^+$ centered charge separated state Fc-ZnPc-$[Cu(phen)_2]^{2+}$-$C_{60}^{\bullet-}$. The intermediate lifetime of 380 ± 90 ns matches the lifetime of the one electron oxidized ZnPc and consequently correlates with the ZnPc-centered charge separated state Fc-ZnPc$^{\bullet+}$-$[Cu(phen)_2]^+$-$C_{60}^{\bullet-}$. Finally, the longest lifetime associated with the one-electron reduced C_{60} of 4.9 ± 0.7 μs is assigned to the thermodynamically most stable charge separated state, namely Fc$^{\bullet+}$-ZnPc-$[Cu(phen)_2]^+$-$C_{60}^{\bullet-}$. This is consistent with the results obtained for rotaxane **1**.
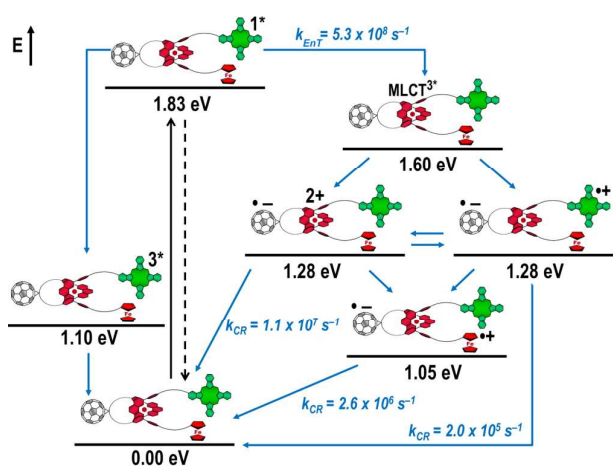
Journal Name

ARTICLE

Fig. 14 Left: differential absorption spectra (visible and near infrared) registered upon nanosecond flash photolysis (670 nm, 5 mJ) of Fc-ZnPc-[Cu(phen)$_2$]$^+$-C$_{60}$ rotaxane **3** under aerobic conditions in tetrahydrofuran with time delays between 9 ns (purple) and 2.0 μs (wine) at room temperature. Inset: zoom into the near infrared region after 200 ns. Right: differential absorption spectra (near infrared) registered upon nanosecond flash photolysis (670 nm, 5 mJ) of Fc-ZnPc-[Cu(phen)$_2$]$^+$-C$_{60}$ rotaxane **3** under aerobic conditions in tetrahydrofuran with time delays between 9 (purple) and 50 ns (green) at room temperature.

Fig. 15 Time absorption profiles of Fc-ZnPc-[Cu(phen)$_2$]$^+$-C$_{60}$ rotaxane **3** upon 670 nm excitation in tetrahydrofuran at room temperature under aerobic conditions at 830 nm (left) and 1010 nm (center and right), monitoring the charge recombination.

Fig. 16 schematically outlines the excitation and deactivation pathways in rotaxane **3**. When exciting directly into the ZnPc Q-bands at 670 nm or into the ZnPc Soret band at 387 nm, the ZnPc singlet excited state is generated, with an energy of 1.83 eV relative to the ground state. Deactivation processes include fluorescence with a quantum yield of 15% and ISC to give the triplet excited state of ZnPc (~ 1.1 eV) followed by the triplet signature in the ns-transient absorption spectra (~ 500 nm). Deactivation occurs via energy transfer to [Cu(phen)$_2$]$^+$, which is confirmed by 50 % quenching of the ZnPc emission (Table S2). Spectroscopically only the ^{3}MLCT* (~ 1.6 eV) state can be resolved, since the ^{1}MLCT* is only stable for several hundreds of femtoseconds.[58, 59] Electron transfer takes place from the ^{3}MLCT* state to generate the charge separated state Fc-ZnPc-[Cu(phen)$_2$]$^{2+}$-C$_{60}$$^{•-}$ with a lifetime of 88 ns (k_{CR} = 1.1 10^7 s^{-1}). This state has been identified from the signature of the one-electron reduced C$_{60}$ at 1010 nm (Fig. 14 and 15). Furthermore, two additional lifetimes were found for the C$_{60}$$^{•-}$. Thus, we conclude

that from the state Fc-ZnPc-[Cu(phen)$_2$]$^{2+}$-C$_{60}$$^{•-}$ a charge shift occurs to form the ZnPc- and Fc-centered charge separated states, which are stable for 380 ns (k_{CR} = 2.6 x 10^6 s^{-1}) and 4.9 μs (k_{CR} = 2.0 10^5 s^{-1}), respectively. From the present data, it has been impossible to verify with certainty whether the two charge shift processes take place simultaneously or successively. The assignment of the lifetimes from the 1010 nm decay has been made by comparison with the one electron oxidized ZnPc$^{•+}$ decay at ~ 830 nm, and by comparison with the charge separated state lifetimes found for rotaxanes **1** and **2**. Considering the energy levels of the three different charge separated states, Fc-ZnPc-[Cu(phen)$_2$]$^{2+}$-C$_{60}$$^{•-}$ and Fc-ZnPc$^{•+}$-[Cu(phen)$_2$]$^+$-C$_{60}$$^{•-}$ seem to exhibit the same energy level, i.e. 1.28 eV, while the Fc$^{•+}$-ZnPc-[Cu(phen)$_2$]$^+$-C$_{60}$$^{•-}$ charge separated state at 1.05 eV is thermodynamically most stable.

Fig. 16 Schematic energy level diagrams, proposed decay pathways and rate constants for Fc-ZnPc-[Cu(phen)$_2$]$^+$-C$_{60}$ rotaxane **3** upon excitation at 670 nm. k_{EnT} = energy transfer rate k_{CR} = charge recombination rate. Energy levels not to scale.

Conclusion

It is evident that all three of the newly investigated donor-acceptor rotaxanes undergo similar deactivation pathways upon photoexcitation. The differences become obvious when looking at the charge separated state lifetimes. The [Cu(phen)$_2$]$^+$ centered charge separated (CS) states feature lifetimes shorter than 100 ns, while the corresponding ZnPc - centered CS state in rotaxanes **2** and **3** exhibit lifetimes in the range of several hundreds of nanoseconds. Although the ZnP centered CS state is energetically at a similar level as those centered at the [Cu(phen)$_2$]$^+$ complex and ZnPc (~ 1.3 eV), considerably longer lifetimes (in the microsecond time regime) are observed for the former. In case of the [Cu(phen)$_2$]$^+$-centered charge separated sate, the shorter lifetimes arise from shorter distances between the radical ions, while ZnPc is generally known to form shorter lived radical ion pairs with C$_{60}$ than ZnP, since smaller energy gaps for the back electron transfer step pulls these processes closer to the top of the Marcus parabola.[1, 60] The longest lifetimes determined are for the energetically favored Fc-centered CS state (~ 1.1 eV). However, in rotaxane **1**, the lifetime (61 μs) is considerably longer than for rotaxane **3** (4.9 μs). Thus, it is concluded that the Fc$^{•+}$-C$_{60}$$^{•-}$ CS state is better stabilized by ZnP (rotaxane **1**) than by ZnPc (rotaxane **3**).

In comparison to previously studied (pseudo-)rotaxanes incorporating either ZnPc,[61] Fc,[16] or ZnP,[14, 15, 18] significantly longer charge separated state lifetimes have been achieved in the new rotaxanes **1**, **2**, and **3**. For example, in ferrocene stoppered [Cu(phen)$_2$]$^+$-C$_{60}$ rotaxanes only the (Fc)$_2$-[Cu(phen)$_2$]$^{2+}$-C$_{60}$$^{•-}$ charge separated state with a lifetime of 15-16 ns (k_{CR} = 6.3 - 6.7 x 10^7 s^{-1}) was observed, without any appreciable evidence for a subsequent charge shift to the ferrocene units.[16] However, when replacing one of the Fc stoppers by ZnP (rotaxane **1**) or ZnPc (rotaxane **3**), a charge shift from ZnP and ZnPc to the ferrocene takes place to yield the thermodynamic more stable Fc–centered charge separated states, with lifetimes in the microsecond regime. In our previously reported C$_{60}$-stoppered porphyrino-rotaxanes, a long lived ZnP$^{•+}$-[Cu(phen)$_2$]$^+$-(C$_{60}$)$_2$$^{•-}$ of 32 μs lifetime (k_{CR} = 3.1 x 10^4 s^{-1}) were detected.[14] How-

ever, when combining the virtues of ZnP and Fc as electron donors, as in the present work, charge separated states with almost twice the lifetime are achievable. Therefore, the combination in a single [Cu(phen)$_2$]$^+$-based rotaxane system of the outstanding electrochemical and spectroscopic properties of ZnP with the low oxidation potential of ferrocene and the extraordinary electron accepting properties and low reorganization energy of C$_{60}$ yields very attractive photoactive materials capable of absorbing light over a very wide range of the visible spectrum and undergoing a cascade of energy and electron transfer processes that ultimately produce charge separated states with lifetimes in the microsecond time domain.

Notes and references

1   S. Kirner, M. Sekita and D. M. Guldi, *Adv. Mater.*, 2014, **26**, 1482-1493.
2   P. L. Anelli, P. R. Ashton, R. Ballardini, V. Balzani, M. Delgado, M. T. Gandolfi, T. T. Goodnow, A. E. Kaifer, D. Philp, P. Marek, L. Prodi, M. V. Reddington, A. M. Z. Slawin, N. Spencer, J. F. Stoddart, C. Vicent and D. J. Williams, *J. Am. Chem. Soc.*, 1992, **114**, 193-218.
3   P. R. Ashton, V. Balzani, A. Credi, O. Kocian, D. Pasini, L. Prodi, N. Spencer, J. F. Stoddart, M. S. Tolley, M. Venturi, A. J. P. White and D. J. Williams, *Chem. Eur. J.*, 1998, **4**, 590-607.
4   P. R. Ashton, T. T. Goodnow, A. E. Kaifer, M. V. Reddington, A. M. Z. Slawin, N. Spencer, J. F. Stoddart, C. Vicent and D. J. Williams, *Angew. Chem. Int. Ed. Engl.*, 1989, **28**, 1396-1399.
5   J. D. Megiatto, Jr., A. Antoniuk-Pablant, B. D. Sherman, G. Kodis, M. Gervaldo, T. A. Moore, A. L. Moore and D. Gust, *Proc. Natl. Acad. Sci. U S A*, 2012, **109**, 15578-15583.
6   J. D. Megiatto, Jr., D. D. Mendez-Hernandez, M. E. Tejeda-Ferrari, A. L. Teillout, M. J. Llansola-Portoles, G. Kodis, O. G. Poluektov, T. Rajh, V. Mujica, T. L. Groy, D. Gust, T. A. Moore and A. L. Moore, *Nat Chem*, 2014, **6**, 423-428.
7   Y. Zhao, J. R. Swierk, J. D. Megiatto, Jr., B. Sherman, W. J. Youngblood, D. Qin, D. M. Lentz, A. L. Moore, T. A. Moore, D. Gust and T. E. Mallouk, *Proc. Natl. Acad. Sci. U S A*, 2012, **109**, 15612-15616.
8   L. Kálmán, R. LoBrutto, J. P. Allen and J. C. Williams, *Nature*, 1999, **402**, 696-699.
9   X. Lin, H. A. Murchison, V. Nagarajan, W. W. Parson, J. P. Allen and J. C. Williams, *Proc Natl Acad Sci USA*, 1994, **91**, 10265-10269.
10   P. L. Dutton and C. C. Mosser, *Proc. Natl. Acad. Sci. USA*, 1994, **91**, 10247-10250.
11   J. D. Megiatto, Jr., D. I. Schuster, S. Abwandner, G. de Miguel and D. M. Guldi, *J. Am. Chem. Soc.*, 2010, **132**, 3847-3861.
12   J. D. Megiatto, Jr., D. I. Schuster, G. de Miguel, S. Wolfrum and D. M. Guldi, *Chem. Mater.*, 2012, **24**, 2472-2485.
13   J. D. Megiatto, Jr., R. Spencer and D. I. Schuster, *J. Mater. Chem.*, 2011, **21**, 1544.
14   K. Li, P. J. Bracher, D. M. Guldi, M. A. Herranz, L. Echegoyen and D. I. Schuster, *J. Am. Chem. Soc.*, 2004, **126**, 9156-9157.

15   K. Li, D. I. Schuster, D. M. Guldi, M. A. Herranz and L. Echegoyen, *J. Am. Chem. Soc.*, 2004, **126**, 3388-3389.

16   J. D. Megiatto, Jr., K. Li, D. I. Schuster, A. Palkar, M. A. Herranz, L. Echegoyen, S. Abwandner, G. Miguel and D. M. Guldi, *J. Phys. Chem. B*, 2010, **114**, 14408-14419.

17   J. D. Megiatto, Jr., R. Spencer and D. I. Schuster, *Org. Lett.*, 2009, **11**, 4152-4155.

18   D. I. Schuster, K. Li, D. M. Guldi and J. Ramey, *Org. Lett.*, 2004, **6**, 1919-1922.

19   L. Flamigni, A. M. Talarico, J. C. Chambron, V. Heitz, M. Linke, N. Fujita and J. P. Sauvage, *Chem. Eur. J.*, 2004, **10**, 2689-2699.

20   C. O. Dietrich-Buchecker and J.-P. Sauvage, *Tetrahedron Lett.*, 1983, **24**, 5095-5098.

21   C. O. Dietrich-Buchecker and J.-P. Sauvage, *J. Am. Chem. Soc.*, 1984, **106**, 3043-3045.

22   C. O. Dietrich-Buchecker and J.-P. Sauvage, *Chem. Rev.*, 1987, **87**, 795-810.

23   C. O. Dietrich-Buchecker and J.-P. Sauvage, *Tetrahedron*, 1990, **46**, 503-512.

24   J.-P. Sauvage and C. O. Dietrich-Buchecker, *Molecular Catenanes, Rotaxanes and Knots*, Wiley VCH, Weinheim, Germany, 1999.

25   J. D. Megiatto, Jr. and D. I. Schuster, *Org. Lett.*, 2011, **13**, 1808-1811.

26   M. Andersson, M. Linke, J.-C. Chambron, J. Davidsson, V. Heitz, J.-P. Sauvage and L. Hammarström, *J. Am. Chem. Soc.*, 2000, **122**, 3526-3527.

27   M. Linke, J.-C. Chambron, V. Heitz and J.-P. Sauvage, *J. Am. Chem. Soc.*, 1997, **119**, 11329-11330.

28   J. S. Lindsey, *Acc. Chem. Res.*, 2010, **43**, 300-311.

29   E. M. Maya, P. Vázquez and T. Torres, *Chem. Eur. J.*, 1999, **5**, 2004-2013.

30   J. D. Megiatto, Jr. and D. I. Schuster, *Chem. Eur. J.*, 2009, **15**, 5444-5448.

31   J. P. C. Tomé, A. M. V. M. Pereira, C. M. A. Alonso, M. G. P. M. S. Neves, A. C. Tomé, A. M. S. Silva, J. A. S. Cavaleiro, M. V. Martínez-Díaz, T. Torres, G. M. A. Rahman, J. Ramey and D. M. Guldi, *Eur. J. Org. Chem.*, 2006 **1**, 257-267.

32   S. FitzGerald, C. Farren, C. F. Stanley, A. Beeby and M. R. Bryce, *Photochem. Photobiol. Sci.*, 2002, **1**, 581-587.

33   S. V. Kirner, D. M. Guldi, J. D. Megiatto, Jr. and D. I. Schuster, *Nanoscale*, 2015, **7**, 1145-1160.

34   T. Kato, T. Kodama, T. Shida, T. Nakagawa, Y. Matsui, S. Suzuki, H. Shiromaru, K. Yamauchi and Y. Achiba, *Chem. Phys. Lett.*, 1991, **180**, 446-450.

35   S. A. Vail, P. J. Krawczuk, D. M. Guldi, A. Palkar, L. Echegoyen, J. P. C. Tome, M. A. Fazio and D. I. Schuster, *Chem. Eur. J.*, 2005, **11**, 3375-3388.

36   L. Pekkarinen and H. Linschitz, *J. Am. Chem. Soc.*, 1960, **82**, 2407-2411.

37   T. Kato, *Laser Chem.*, 1994, **14**, 155-160.

38   D. M. Guldi, M. Maggini, G. Scorrano and M. Prato, *J. Am. Chem. Soc.*, 1997, **119**, 974-980.

39   H. Imahori, H. Norieda, H. Yamada, Y. Nishimura, I. Yamazaki, Y. Sakata and S. Fukuzumi, *J. Am. Chem. Soc.*, 2001, **123**, 100-110.

40   H. Imahori, K. Tamaki, D. M. Guldi, C. Luo, M. Fujitsuka, O. Ito, Y. Sakata and S. Fukuzumi, *J. Am. Chem. Soc.*, 2001, **123**, 2607-2617.

41   H. Imahori, H. Yamada, Y. Nishimura, I. Yamazaki and Y. Sakata, *J. Phys. Chem. B*, 2000, **104**, 2099-2108.

42   F. Spanig, C. Kovacs, F. Hauke, K. Ohkubo, S. Fukuzumi, D. M. Guldi and A. Hirsch, *J. Am. Chem. Soc.*, 2009, **131**, 8180-8195.

43   D. Gonzalez-Rodriguez, T. Torres, M. M. Olmstead, J. Rivera, M. A. Herranz, L. Echegoyen, C. A. Castellanos and D. M. Guldi, *J. Am. Chem. Soc.*, 2006, **128**, 10680-10681.

44   D. M. Guldi, *Chem. Soc. Rev.*, 2002, **31**, 22-36.

45   C. Grewer and H.-D. Brauer, *J. Phys. Chem.*, 1994, **98**, 4230-4235.

46   R. A. Marcus, *Angew. Chem.*, 1993, **105**, 1161-1172.

47   G. Grampp, *Angew. Chem. Int. Ed.*, 1993, **32**, 691-693.

48   D. M. Guldi, *Chem. Commun.*, 2000, 321-327.

49   C. Luo, D. M. Guldi, H. Imahori, K. Tamaki and Y. Sakata, *J. Am. Chem. Soc.*, 2000, **122**, 6535-6551.

50   D. M. Guldi, A. Gouloumis, P. Vázquez and T. Torres, *Chem. Commun.*, 2002, 2056-2057.

51   A. Hausmann, A. R. Soares, M. V. Martinez-Diaz, M. G. Neves, A. C. Tome, J. A. Cavaleiro, T. Torres and D. M. Guldi, *Photochem. Photobiol. Sci.*, 2010, **9**, 1027-1032.

52   A. M. V. M. Pereira, A. R. M. Soares, A. Hausmann, M. G. P. M. S. Neves, A. C. Tomé, A. M. S. Silva, J. A. S. Cavaleiro, D. M. Guldi and T. Torres, *Phys. Chem. Chem. Phys.*, 2011, **13**, 11858.

53   M. Quintiliani, A. Kahnt, T. Wolfle, W. Hieringer, P. Vazquez, A. Gorling, D. M. Guldi and T. Torres, *Chem. Eur. J.*, 2008, **14**, 3765-3775.

54   W. Seitz, A. Kahnt, D. M. Guldi and T. Torres, *J. Porphyrins Phthalocyanines*, 2009, **13**, 1034-1039.

55   R. F. Enes, J. J. Cid, A. Hausmann, O. Trukhina, A. Gouloumis, P. Vazquez, J. A. Cavaleiro, A. C. Tome, D. M. Guldi and T. Torres, *Chem. Eur. J.*, 2012, **18**, 1727-1736.

56   A. J. Jimenez, M. L. Marcos, A. Hausmann, M. S. Rodriguez-Morgade, D. M. Guldi and T. Torres, *Chem. Eur. J.*, 2011, **17**, 14139-14146.

57   A. M. Pereira, A. Hausmann, A. R. Soares, J. P. Tome, O. Trukhina, M. Urbani, M. G. Neves, J. A. Cavaleiro, D. M. Guldi and T. Torres, *Chem. Eur. J.*, 2012, **18**, 3210-3219.

58   N. Armaroli, M. A. J. Rodgers, P. Ceroni, V. Balzani, C. O. Dietrich-Buchecker, J.-M. Kern, A. Bailal and J.-P. Sauvage, *Chem. Phys. Lett.*, 1995, **241**, 555-558.

59   T. Gunaratne, M. A. J. Rodgers, D. Felder, J.-F. Nierengarten, G. Accorsi and N. Armaroli, *Chem. Commun.*, 2003, 3010.

60   G. Bottari, G. de la Torre, D. M. Guldi and T. Torres, *Chem. Rev.*, 2010, **110**, 6768-6816.

61   D. M. Guldi, J. Ramey, M. V. Martínez-Díaz, A. de la Escosura, T. Torres, T. Da Ros and M. Prato, *Chem. Commun.*, 2002, 2774-2775.